UNIVERSITY OF
KWAZULU-NATAL

INYUVESI
YAKWAZULU-NATALI

WIND TUNNEL SIMULATIONS TO DETECT AND QUANTIFY THE TURBULENT EFFECTS OF A PROPAGATING HE-NE LASER BEAM IN AIR

SHIVAN MICHAEL AUGUSTINE

2016

WIND TUNNEL SIMULATIONS TO DETECT AND QUANTIFY THE TURBULENT EFFECTS OF A PROPAGATING HE-NE LASER BEAM IN AIR

by

Shivan Michael Augustine

209506040

BSc Hons (Physics)

MSc Physics

Submitted in partial fulfillment of the requirements

for the degree of Doctor of Philosophy in the

School of Chemistry and Physics,

University of KwaZulu-Natal

Pietermaritzburg

Contents

List of Figures

Declaration

This dissertation describes the work undertaken in the School of Chemistry and Physics, University of KwaZulu-Natal (Pietermaritzburg), under the supervision of Prof. N. Chetty, between June 2014 and November 2016. I declare this to be my original work except where due reference and credit is given.

Student: Mr Shivan Michael Augustine

Signature: .....

Date: .....

Supervisor: Professor Naven Chetty

Signature: .....

Date: .....

Acknowledgments

- I wish to thank God for giving me the strength, courage and support throughout my studying years. I am forever and always grateful to you.

- To my supervisor, Prof. N. Chetty, thank you for your guidance and support throughout this work. It has been an amazing learning experience with you and I am forever grateful for the time you have given in this regard.

- To my wife, Eurika Augustine, your patience, support, love and care has been everything I could have asked for. I thank you for everything you have done for me during this work.

- Thanks goes to the NRF and CSIR for awarding me scholarships throughout my PhD.

- Lastly, I wish to extend my gratitude to my closest friends and family for their support and well wishes.

SUMMARY

In this work, we set out to determine the effectiveness of using a point diffraction interferometer (PDI) as the detection source for a laser beam propagating through a heated wind tunnel. The technique we used was previously developed by Ndlovu and Chetty in 2014 and improved upon by Augustine and Chetty in 2015. We use the same technique with new additions and adjustments. The experiment was carried out as follows. We considered a He-Ne laser beam having the characteristics of being Gaussian, coherent and monochromatic. By propagating the laser beam through the turbulent medium, the beam was exposed to an inhomogeneous medium which was riddled with variating eddy currents. Research has shown that each eddy is unique in its shape and form and hence will perturb the beam in a random fashion. Laboratory experiments were setup to establish the extent of these effects. Amongst the measured parameters of temperature, pressure and wind speed, the experiment yielded interferograms which were analysed using statistical software. Inspection of the resultant interferograms have shown signs of a loss in coherence, intensity, shape and form. Further analysis has been described in Chapter 5.

Our results have shown to coincide well with published works whilst being developed on a much smaller scale. The setup has successfully shown to be highly robust and cost efficient. Such benefits make this setup unique and pave the way for further upgrades/development. Future work entails developing a heated water bath which will represent a new turbulence source. In addition, we look to

upgrading the laser used in this work so as to gather an understanding of how different lasers behave under similar conditions. These results will assist in creating a larger repository of knowledge for understanding the atmosphere as well as the behaviour of laser beams propagating through them. With the variety of laser applications existing in this day and age, it is of utmost importance to study their nature and hence be able to build suitable models to replicate real world conditions and behaviour.

Thesis Structure

Chapter 1 contains the background theory of the atmosphere. We review past and current literature and provide insight into the vast applications of lasers in the real world.

Chapter 2 presents the theory of atmospheric turbulence. The effects of laser beams on the atmosphere are explored and reviewed. An elaboration of the impact of turbulence on laser beam propagation is provided. The effects of aerosols on the atmosphere is also discussed. The field of interferometry is discussed together with a quick review of the PDI.

Chapter 3 provides the experimental design and analysis used to achieve the results and a description of the inhibiting factors experienced during simulations and this work in general.

Chapter 4 presents the challenges faced during the period of this work.

Chapter 5 presents the accepted journal article to ATMÓSFERA on 20 October 2016 in the required format. In this paper, simulations were conducted to measure the turbulent effects experienced by a laser beam propagating through a heated wind tunnel. In addition to a variety of characteristics being measured, we set out to establish the effectiveness of using a point diffraction interferometer in being able to detect and fully quantify the turbulent effects.

List of Abbreviations and Symbols

A - Total ring area of the gyroscope

ABL - Atmospheric boundary layer

c - Speed of light

c_p - Specific heat capacity of water

CO_2 - Carbon dioxide

C_n^2 - Refractive index structure function $(\mathrm{m}^{-2/3})$

C_T^2 - Temperature structure function $(\mathrm{K}^2\mathrm{m}^{-2/3})$

cw - continuous wave

°C - Degrees Celcius ($°C$)

d - Average layer thickness (m)

D_s - Phase structure function

D_T - Differential temperature

D_μ - Diffusion coefficient

f - Frequency (Hz)

$F_1/F_2/f_1/f_2$ - Focal distances of two lenses

FBH - Ferdinand-Braun-Institute

FFT - Fast Fourier transform

H - Latent heat

He-Ne - Helium Neon

I - Intensity

k/K - Wavenumber (nm)

L - Propagation path length (m)

l - Size of the eddy

l_0 - Inner scale of turbulence

L_0 - Outer scale of tubulence

LASER - Light Amplification by Stimulated Emission of Radiation

LIDAR - Light detection and ranging

n - Refractive index

OCT - Optical coherence tomography

p/P - Pressure (kPa)

P_g - Perimeter of the gyroscope

PDI - Point diffraction interferometer

q - Energy spent in raising the temperature by a unit volume of the material

r - Length between two reference points (m)

$\vec{r_1}$ - Position vector

R_e - Reynolds number (dimensionless)

R(z) - Radius of the curvature of the phase front

r_0 - Fried's parameter (cm)

T - Temperature (K)

u - Mean velocity $(\mathrm{m.s}^{-1})$

UV - Ultra violet

w(z) - Beam radius

w_0 - Beam waist

Z_R - Rayleigh range

ν - Kinematic viscosity $(\mathrm{m}^2.\mathrm{s}^{-1})$

Φ_n - Power spectral density

$\phi(\overline{K})$ - Velocity spectrum

Φ - Phase of perturbed wavefront

$\vec{\kappa}$ - Wavenumber vector

κ - Wavenumber (nm)

σ - Distance traveled by the laser beam

δ - Real displacement (cm)

λ - wavelength of the laser beam (nm)

β - Backscatter coefficient

Ω - Rotation velocity of the gyroscope

ψ - Laser cutting speed (ms)

α - Absorption coefficient

ρ - Density of water

Chapter 1

INTRODUCTION

1.1 Background

Atmospheric optics involves studying the way in which the atmosphere reacts with light. It is one of the most important aspects in optics and therefore research is highly sought after by scientists all around the world. The interaction of light with the atmosphere can be through a number of ways, namely absorption, refraction, reflection, transmission and emission [1]. The enabling factor for these processes are through the molecules that exist within the air. The number of molecules in the air at any given point vary in space and time and generally decrease relative to altitude. To better understand the interactions between molecules and the atmosphere, an analysis of the atmosphere is necessary.

The atmosphere is divided into two major categories. Figure (1.1) provides a graphic view of the two layers in relation to height above ground. The first layer is the atmospheric boundary layer (ABL) and the second, the free atmosphere.

The first 200 meters of the ABL represents the most unstable portion of the atmosphere since surface heating leads to surface convection, thermal plumes and severe turbulence. Molecules in the air rise and fall in a stochastic manner which causes any light traveling through it to be affected negatively. Since heating of the earth can happen at different rates, the atmosphere in general is considered to be a highly unstable fluid.

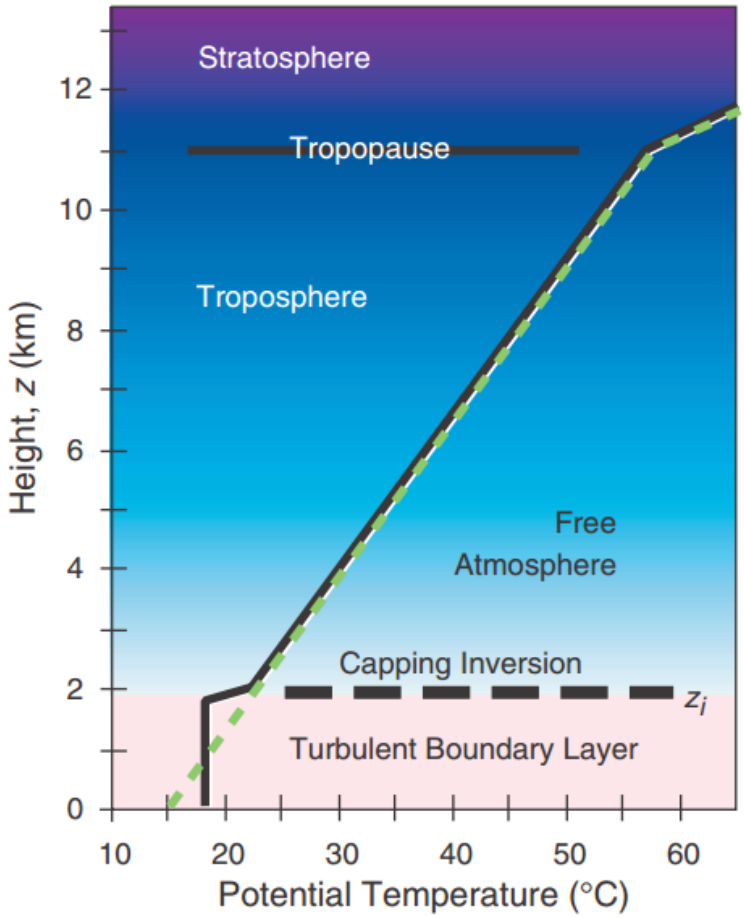

Figure 1.1: Graphic description of the standard atmosphere [2]

Before light enters the Earth's atmosphere its trajectory follows a straight line path. Upon entry, the atmosphere interacts with the light and causes distortion. This phenomena is known as refraction. Various types of refraction exist each having their own unique interference characteristics. Some types are astronomical,

atmospheric, cosmic and random refraction [3].

The second category of the atmosphere is the free atmosphere and is defined as the region where the surface's inhibiting contributions are negligible and pose minor optical turbulence. Since our study does not consider a free atmosphere, we restrict ourselves to the ABL.

Figure (1.2) provides an example of how thermals rise in a fluid. A similar behaviour can be expected for thermals rising from a heated surface [4]. The rising plumes cause vortices in the air which lead to another phenomena known as eddies. Further explanation will follow in section 1.2.

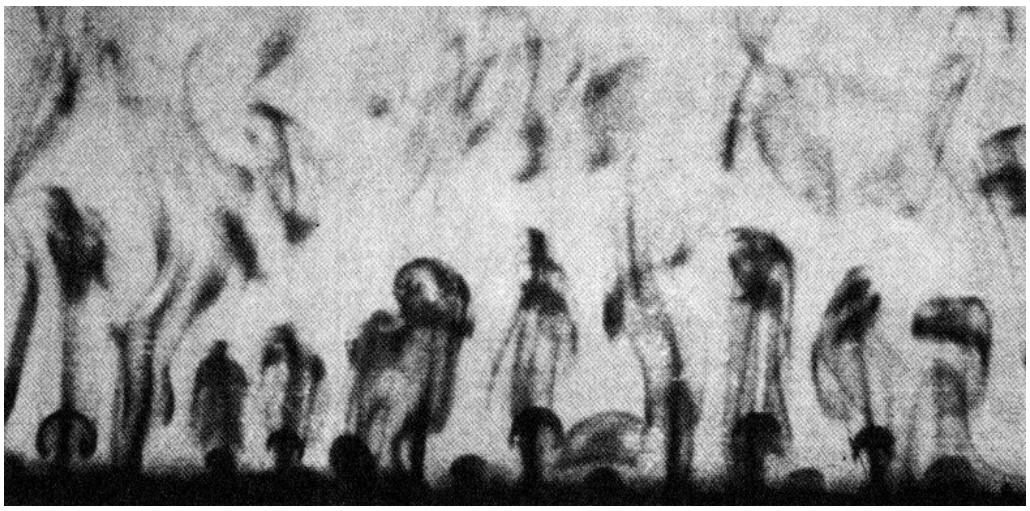

Figure 1.2: Image of thermal plumes rising from a heated surface in a fluid

1.2 Current Literature

The theory of atmospheric turbulence is characterised by the way in which the atmosphere behaves with respect to temperature and pressure. Variations in these

two parameters induce random fluctuations of the refractive index denoted by n [3]. As depicted in Figure (1.2), the atmosphere can be modeled as a series of turbulent eddies each having unique sizes and shapes and each posing a unique refractive index.

The power spectral density function $\Phi_n(\vec{\kappa})$ characterises the relative incidence of the eddies whose dimensions are given by $\left(L_x = \frac{2\,\pi}{\kappa_x}, L_y = \frac{2\,\pi}{\kappa_y}, L_z = \frac{2\,\pi}{\kappa_z}\right)$ and where $\vec{\kappa} = (\kappa_x, \kappa_y, \kappa_z)$ is the wavenumber vector. For homogeneous and isotropic turbulence, the power spectrum places its dependence solely on the scalar quantity, $\kappa = |\vec{\kappa}|$ [5]. Kolmogorovs theory of turbulence distinguishes an inertial subrange which exists for values of κ greater than some critical value of the wavenumber κ_0 while being less than κ_m [6]. Furthermore, the power spectral density can be inferred through the laws of turbulent flow as,

$$\Phi_n(\vec{\kappa}) = 0.033\, C_n^2\, \kappa^{11/3}, \quad \text{where}\, \kappa_0 < \kappa < \kappa_m, \tag{1.1}$$

where, C_n^2 is the refractive index structure function.

As with most atmospheric measurements, the magnitude of the refractive index structure function C_n^2 provides adequate data to determine the nature of the atmosphere [7]. More specifically, C_n^2 can be determined numerically through the equation [3],

$$C_n^2 = \left(79.0 \times 10^{-8} \left[\frac{\mathrm{p}}{\mathrm{T}^2}\right]\right)^2 \mathrm{C}_T^2, \tag{1.2}$$

with

$$C_T^2 = \left(\sqrt{< (\mathrm{T}_1 - \mathrm{T}_2)^2 >}\right) \mathrm{r}^{-1/3}, \tag{1.3}$$

where p is the atmospheric pressure in millibars and <> represents the ensemble average [3]. C_T^2 is defined as the temperature structure function where T_1 and T_2 are two reference points separated by a distance r [3]. The value of C_n^2 depends on geographical location and has been shown to vary from one source to the other, but in general ranges from $10^{-17}\mathrm{m}^{-2/3}$ or less for weak turbulence and $10^{-13}\mathrm{m}^{-2/3}$ or more for strong turbulence [3, 8–13].

Measuring the effects of random variations in n can often be described through the phase structure function given by [14],

$$D_s(\vec{r_1}, \vec{r_2}) = \langle \phi\, \vec{r_1} - \phi\, \vec{r_2} \rangle^2\,, \tag{1.4}$$

where ϕ represents the phase of the perturbed wavefront and $\vec{r_1}$, the position vector and $\langle\rangle$, the ensemble average. By modeling the turbulence using Kolmogorov statistics, the phase structure function will be proportional to $r^{5/3}$ for values of r within the inertial subrange. Since C_n^2 can be estimated through a variety of models, the results can be compared regardless of the method used. Since as early as 1969, turbulence measurements have been carried out by numerous authors [11, 12, 15, 16].

In 1974, Hogge and Visinsky [16] passed a 10 mW He-Ne laser beam into the highly turbulent flow produced by a jet engine and calculated the refractive

structure constant to be of the order $10^{-5}\,\mathrm{m}^{-2/3}$. Such values represent very strong turbulence which can be expected since temperatures of the jet engines afterburner produced up to 615°C in the air flow. From equation 1.2 and 1.3, it is observed that for high C_T^2, a high C_n^2 can be expected. Hogge and Visinsky [16] compared their work to two other techniques, the first being a measurement of the scintillation of a 10.6 micron beam propagating through the exhaust [17]. The results showed approximate agreement since propagation distances were significantly smaller. Here again, equation 1.2 describes the dependence of the path length on C_n^2. The second technique used two hot wire anemometers to measure the structure constant [18–20]. This was achieved by positioning either anemometer at two reference points within the exhaust flow. For this technique, turbulence measurements could not be achieved since the high flow rate of the exhaust caused the probes to dislodged off the senors. Our turbulence source generated significantly smaller temperature differentials and hence a significantly smaller structure constant can be expected.

Hogge and Visinsky [16] paved the way for Barrett and Budni [15], who in 1992 developed and measured the refractive index structure function within a heated jet stream. The experiment yielded results for the refractive index structure function and provided explanations for beam wander, beam spreading and energy redistributions of a laser beam. Such results have been adapted for the improvement of active imaging, directional infrared counter measures (DIRCM) and communications. Isterling *et al* [21] further investigated the ground work of Barrett and Budni [15], to establish the extent of beam wander and spread on the

previously mentioned applications. They performed a series of experiments using a Gnome jet engine operated at two settings, the first at idle, the second at maximum RPM. The effect of the laser beam propagating through the flow was determined through analysis of the spot images. The findings from their work provided insight into the structure and composition of the turbulent flow at various temperatures and wind speeds. These results were then used to develop corrective measures and improve the lasers application.

The past works of [15, 16, 21] made use of large jet engines to measure their impact on He-Ne laser beams. In addition, propagation was conducted in the open atmosphere which was subject to wind and temperature fluctuations amongst other factors. Various additional works have been conducted by other authors [22–27] and describe various types of experimental setups with the common focus being the refractive index structure function and in some cases, other turbulent characteristics. These sources have been useful in our work since we have a wide range of data available for comparison.

In 1970, a technique known as thermosondes (thermal sensor radiosonde) was first prototyped. The construction entailed using weather balloons fitted with measuring instruments and sensors [28]. This technique proposes a completely different experimental setup since the actual optics and sensors are sent into the atmosphere to measure characteristics as it moves. The balloons were fixed at a set distance apart and measured the vertical profile to very high accuracies. The

differential measurements between the pair of sensors derived the structure function directly through the relation [29],

$$D_T(r) =< [T(x) - T(x+r)]^2 >, \tag{1.5}$$

where D_T represents the differential temperature between the sensors, T the temperature and r the distance between the sensors. Key assumptions however were made in thermosondes, namely that the atmosphere was isotropic and homogeneous. The thermosondes technique also provided data for C_T^2 and therefore C_n^2 was inferred through calculating the mean square temperature fluctuations between two reference points and by using the Obukhov [30]-Kolmogorov [31] turbulence theory [32],

$$C_T^2(h) = \left(\frac{[T(\vec{r_1}) - T(\vec{r_1})]^2}{r^{2/3}} \right), \tag{1.6}$$

where, $r = |\vec{r_2} - \vec{r_1}|$. From equation 1.6, C_n^2 can be determined from,

$$C_n^2(h) = \left[\frac{80.0\, P(h)}{T(h)^2} \times 10^{-6} \right]^2 C_T^2(h), \tag{1.7}$$

where variables have their usual meanings.

The accuracy of this technique is within 10% for the extremes of turbulence and ambient temperature [32]. Thermosondes ability to accomplish vertical profiling with relative ease proved it to be advantageous over other methods such as radar [32]. One of the main disadvatages of thermosondes which prevents its

widespread usage in the measurement of laser beam turbulence has been the cost of equipment needed and the fact that the measurements could only be carried out during specific times due to air space disturbance. Since air balloons can be quite large, aircrafts had to ensure that their paths did not cross the balloons which could have caused a fatal accident.

Soon after the thermosondes technique emerged, further advancements came in the form of radiosondes. Initial implementations of radiosondes were particularly for meteorological measurements however the design was adapted to make turbulence measurements in 1985 by Warnock and Van Zandt [33]. The setup was similar to that of thermosondes but instead of sensors, radio waves were used for measurements. The radio waves were significantly more stable during the measurements and therefore provided data which was more accurate and reliable.

Recent works by Nyobe et al [13] utilise a similar laboratory setup as Augustine and Chetty [34] but with different optics and detectors. Their work has shown the possibility of measuring the directional fluctuations of a laser beam through a turbulent jet. The interference diffraction pattern is measured by an acquisition system of data and thereafter compared with other similar data. Furthermore, they were able to measure the diffusion coefficients through the relation,

$$D_{\mu} = \frac{(\overline{n})}{4\,\sigma\,D^2}\left(\frac{F1}{f1}\frac{f2}{F2}\right)^2 \overline{\delta}^2, \tag{1.8}$$

where, $\overline{n}$ is the mean value of the refractive index, σ, the distance traveled by the laser beam, δ, the real displacement of the central fringe in the interference pattern and (F_1, F_2, f_1, f_2) are the focal distances of each lens.

In 2015, Ndlovu and Chetty [35] modeled the behaviour of a laser beam traversing through a flame. The setup was not only successful in its implementation but also provided a new means of measuring and quantifying turbulence in air. The results published in their paper has also shown to coincide well with the works of Augustine and Chetty [34] who used a similar setup with modifications. Here the work entailed using a heated panel which mimicked the surface of a road or even the surface of a car on a hot day [34]. The results provided data on how a laser beam behaves through convective perturbations alone. The results faired well with that of Ndlovu and Chetty [35] and provided some insight into classifying directional perturbations using a point diffraction interferometer.

An interesting alternative has been shown by Carnevale [36, 37] where numerical approaches were used to model turbulence and later confirmed through experimental means. With the recent improvement of simulation and modeling capabilities, Carnevale [36,37] has provided new methods and data for determining uncertainties in turbulent flow. In this work, we ignored the effects explained by Carnevale [36,37] as the temperature and velocity of the air flows were not strong enough to create these conditions however any further work in this respect would need to account for these effects.

1.3 Applications of propagating laser beams

1.3.1 Engineering

Ballistic missile detection

The United States air force has developed an airborne laser (ABL) called the YAL-1A which is fitted to the Boeing 747 aircraft for the destruction of ballistic missiles [38]. Figure (1.3) is an image of the actual Boeing 747 with the laser modifications. The front of the aircraft is known as the nose and has on it a built in turret which contains the main laser. Before this laser can fire, many other factors are taken into consideration.

Infrared lasers along the body of the aircraft are used for detection of the missiles and rely on the hot exhaust fumes emitted by the missiles during their boost phase [38]. Once a missile has been detected, a series of low powered lasers will then calculate its distance, speed, air turbulence and course [38]. To compensate for air turbulence errors, the ABL uses adaptive optics to reduce the effects [38].

Once the target has been identified, the high powered laser emits highly focused energy for 3 to 5 seconds at a time [38]. The energy is then transferred from the beam to the target. This causes the missile to heat very quickly and results in failure of its electronics [38].

Figure 1.3: Image of a Boeing 747 with the defense laser system [39]

There are two main advantages of using lasers in these applications. The first is that lasers can be used out of the visible spectrum making them invisible to the human eye. This ensures that the enemy cannot preempt the attack [40, 41]. Secondly, they are silent in their implementation which is advantageous since conventional methods such as firearms and missiles are noisy and can draw attention [40, 41].

Laser weapons can have devastating results if used for attacking purposes. Other countries are aware of this and have started developing countermeasures. China for instance is now developing high tech coatings for defense against laser weapons [42]. The coatings will provide safety in the event of a laser attack by deflecting, reflecting or absorbing the energy. The large cost of developing a laser weapon is far greater than developing a defense for them. Hence China has found this to be a more viable solution [42]. A disadvantage of this countermeasure is that different lasers require different coatings. Developing such a material which could resist any laser would solve this problem. However, at this time such a material is still being researched [42].

Laser gyroscope

Laser gyroscopes are used for measuring and maintaining orientation based on the physical principles of angular momentum [43]. Figure (1.4) depicts the design of a gyroscope which incorporates a laser gyroscope in place of the conventional spinning wheel. Two lasers are fitted to a triangular shaped housing, one on a short end and the other on the long end. When the gyroscope is at rest, both the beams will travel through the same optical path. Once the gyroscope rotates, a phenomena known as the Sagnac effect occurs. This is where each beam sees a different cavity length [43]. The implication of this phenomena results in a frequency difference between the two laser beams. The frequency can be calculated according to [44],

$$\Delta\lambda = \frac{4\,A\,\Omega\,\lambda}{c\,P_g}, \tag{1.9}$$

where, A represents the total ring area, Ω, the rotation velocity of the gyroscope, c, the speed of light and P_g, the perimeter of the gyroscope. From this, the change in frequency can be determined as [44],

$$\Delta f = \frac{4\,A\,\Omega}{\lambda\,P_g}. \tag{1.10}$$

The change in frequency yields a time varying phase shift, between the two laser beams. The intensity can therefore be determined by a frequency which is equivalent to Δf as [44],

$$I = I_0\,(1 + \cos(2\,\pi\,\Delta f\,t)) \tag{1.11}$$

Gyroscopes play vital roles in navigation units for aircrafts, ships and high precision instruments. They are also used in race cars, motor bikes, anti-roll devices and robotics. Their use in respect of calculating orientation and rotation makes them invaluable to the field of science and their contributions to modern technology [44].

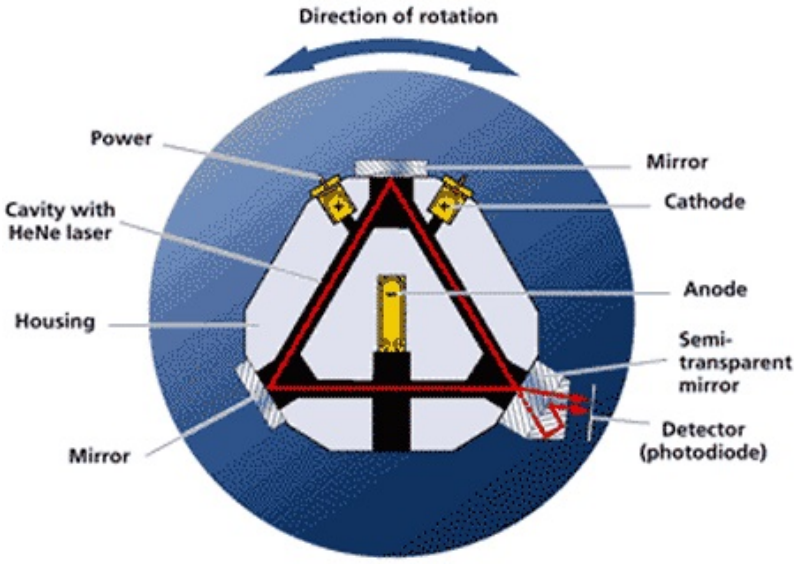

Figure 1.4: Depiction of a ring laser gyroscope [45]

Laser designation

Some military aircrafts use high tech targeting systems which employ lasers for illuminating targets [46]. In this case "illuminated" means that the target is marked for destruction. The aircraft uses an infrared laser to detect the heat signatures from the nearby targets. The infrared laser offers an advantage in this instance, since it transmits over the infrared wavelength which is invisible to the human eye [46]. Once a target has been detected, a series of laser pulses are consistently emitted from the aircraft. These laser pulses create a path from the aircraft to the target which can be identified by the electronics of the missile [46].

The most common types of lasers used to emit the pulses are 850 nm, 1060 nm and 1500 nm. The first two wavelengths are visible at night with the use of night vision goggles. The 1500 nm is invisible even with night vision goggles but are easily detected with short wave infrared cameras. In Figure (1.5), an F-16 fighter jet is seen firing its laser guided missile at a target. The missile will follow the path of the pulses to the target and inevitably destroy it. Such technology is extremely useful when visibility is limited or when the target is moving about randomly [46].

Figure 1.5: An F-16 fighter jet firing its laser guided missile at a target [47]

1.3.2 Medical

Eye Surgery

In the medical field, the use of excimer lasers are becoming more prominent since they provide numerous advantages due to their high level of adjustability and precision [48]. By focusing a highly collimated excimer laser beam to a pin point, a single point of high energy can be used for cutting, burning, sealing or cauterizing. Many procedures often use lasers particularly in delicate operations. This includes

eye surgeries or surgeries which involve organs rich in blood [48]. The cauterizing effects of the laser assists in making clean cuts and this avoids the wounds from bleeding out. Other applications include cancer treatment, dermatology, medical imaging and ophthalmology [49]. Knowledge of how the laser targets different layers of tissue or any matter for this instance could mean the difference between life and death [50, 51].

A common procedure conducted using the excimer laser is LASIK. Conventional methods involve using a blade to operate on the eye which pose significant dangers since the procedure is very delicate [52]. Excimer lasers are very precise and are controlled using computers. They offer more reliable results while being safer to use. The procedure entails creating an opening in the cornea as seen in Figure (1.6). Once the cornea has been opened, the laser can be used to reshape it and correct the refractive error [52].

The cornea can vary in its depth, thus knowledge of this is imperative. The ablation depth can be calculated by Munnerlyn's formula as [52],

$$\text{depth (microns)} = \frac{(\text{diameter of the optical area (mm)})^2 \times \text{dioptric correction}}{3}. \tag{1.12}$$

The ablation depth varies according to the barometric pressure and room temperature. Therefore, particular care has to be taken before the procedure can be conducted [52].

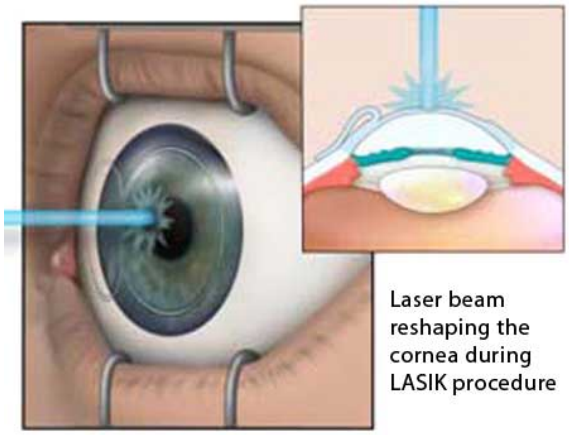

Figure 1.6: Image of lasers used in eye surgery [53]

Optical coherence tomography

Better known as medical OCT, is a noninvasive technique similar to an ultrasound whereby a biological material is mapped below the surface to develop a cross-sectional image [54, 55]. The technique uses a low coherence laser to penetrate the sub-levels of the biological tissue. Scattered light reflects back to the receiver to create an image which defines the various levels of the material [54]. In comparison to other methods such as X-Ray, magnetic resonance imaging and ultrasound imaging, laser OCT is much safer since there is less radiation exposure to the material [55]. This can be highly beneficial in some instances since some materials can degrade under high levels of radiation [54]. The produced images have also shown to be less cloudier and clearer in comparison to other techniques. This means that a correct diagnoses is more probable in OCT [55]. In addition, if the image provides adequate data, the need to perform invasive operations may also be reduced.

1.3.3 Astronomical

Observations

Astronomical observations make use of lasers to map out entire regions in space. Remote sensing techniques make use of lasers for tracking or surveillance [56]. A well known instance of lasers being used for ranging was when Apollo 11 and Apollo 14 landed on the Moon. Astronauts placed retro-reflectors on the moon which can be used to reflect light. By shining a powerful laser from Earth onto the reflectors, the time for the reflection to return can be measured and used to calculate the distance through the equation [57],

$$\text{distance} = \frac{\text{speed of light} \times \text{total time for light to reflect}}{2} \tag{1.13}$$

Using equation 1.13, the average distance to the moon has been calculated to be approximately 385 000 km. Many factors influence the result, some of which are Earth's rotation, weather and air turbulence. Lunar ranging is one of many different types of laser ranging. The common feature between each technique is to measure the amount of light returning from the target and thereafter either drawing conclusions or calculating results. The difference comes in the type of laser used and the way in which it is implemented.

Another useful technique known as satellite laser ranging (SLR) is used to measure the distance between Earth and the satellites that orbit it [57]. The results provide data on the satellites orbit paths as well as other geophysical characteristics.

The process is similar to lunar ranging since a laser is used to transmit pulses at a set time to a satellite, which is equipped with retro-reflectors. The reflection of the laser light is measured by a receiver which also records the time. The data can then be used to calculate the satellites distance and hence create a map of its path [57]. Over time, the technology used to conduct SLR has improved and in turn, improved the accuracy of the results. The use of higher powered lasers, adaptive optics and better computing simulations have brought the accuracy of SLR from a meter level to a centimeter level [57]. The ability to accurately measure distances over time allows for other benefits as well such as the ability to measure Earth's gravitational field, the movement of glaciers, sea level and weather patterns.

1.3.4 Industrial

Laser cutting

A variety of materials can be cut using laser systems-some of which include plastics, textiles, wood and metal. Some lasers have extremely high power ratings, of up to a few hundred watts and have the ability to vaporise metal [58]. In industry, automotive companies make use of carbon dioxide lasers to cut or weld metals. The extremely high intensity of lasers often prove to be much more efficient and precise in their implementation than conventional welding methods. Other industry applications include laser drilling and laser marking [58].

Figure (1.7) illustrates a scenario where a CO_2 laser is used to cut specific shapes in a thick piece of metal. It can be seen that the laser is housed within

the machinery to ensure that the focus is precise. It also protects the laser from any feedback which could come from the metal or other external factors. The high powered beam focuses its light on a single point which heats the metal to a very high temperature. Depending on thickness, the metal will either melt or vaporise. The power of the laser to be used depends on the type of material being cut. The speed at which a laser will cut a material can be determined from [59],

$$\psi = \frac{I\,\alpha\,d}{q}, \tag{1.14}$$

where, ψ is the cutting speed in milliseconds, I the power of the laser per unit surface area (watt per meter squared), α represents the absorption coefficient of the material, d, the average layer thickness (meters) and q, the energy spent in raising the temperature by a unit volume of the material. The variable q is related to the specific heat capacity and latent heat of vapourisation of water through the relation [59],

$$q = \rho(c_p\,\Delta T + H), \tag{1.15}$$

where, ρ is the density of water (grams per centimeter cubed), c_p the specific heat capacity of water (Joule per kilogram degrees Celcius), H, the latent heat (kilojoule per kilogram) and ΔT, the difference in temperature between the body and the boiling point of water [59].

Figure 1.7: Image of a laser cutting machine [60]

1.3.5 Commercial application

Aesthetic

Commercial applications are generally for aesthetic means where He-Ne lasers of various colors are used to create beautiful displays for entertainment. Common examples of its use are in night clubs, concerts and theme parks. Figure (1.8) provides an illustration of a low powered, divergent He-Ne laser beam being used at an orchestral concert. In this case, it is necessary that the beam diverges and spreads its intensity over a greater surface, since a focused beam can cause eye damage.

Figure 1.8: Lasers used for commercial entertainment [62]

CD and DVD players

The laser disc player was produced in 1978 and it was the first mass market product to include a laser [61]. The laser disc was followed by the compact disc (CD) player in 1982, which till today is the most common format choice for different data types. CD players operate using five main components, the disc, the laser, a photoelectric cell, an electronic circuit and a digital to analog converter.

CD's have a readable layer which contains a number of tracks each having pits and lands. Pits are bumps and lands are flat portions on the tracks which are prearranged depending on the content of the CD. An electric motor spins the CD within its case [61]. A semiconductor laser reads off the pits and lands on the CD from the inside out. As the laser moves out, so does the motor speed up to compensate for the longer distance. The pits scatter the laser light while the lands reflect the light straight back [61]. A photocell is positioned next to the laser. This detects the lands which sends a signal to the electronic unit, with the value 1 [61].

For the instance of a pit being detected, the photoelectric cell will not detect any light and sends the value 0 to the electronic unit. Once the entire disc is scanned, a series of 1's and 0's (binary) will be read and stored. Thereafter, an analog to digital converter will decode the binary into a pattern which can be transformed into a series of electric currents which can then be converted to sound energy [61].

Security

Laser detection is becoming a more commonly used security feature in many homes and businesses, since security lasers are invisible and do not make any noise. A laser beam-interruption system detects and monitors movements wherever they are setup. They are triggered if any of the laser beam paths are broken [63]. Due to the narrow beam width, a laser system can be setup in almost any instance for security measures. The system operates in the following manner; a laser is used as the source of light. A transmitter will operate the laser in terms of the number of times it is fired per second (pulses) and a receiver which measures the light after it traverses the propagation path. A base scenario will be calibrated into the receiver in the form of a time that the laser should take to complete its total journey. In the event that an intruder breaks the laser path, the time recorded by the receiver will be greater than the base scenario. This then will cause an alarm to trip and hopefully deter the intruders. Since lasers will always maintain their basic properties, their application in security will always prove to be successful.

1.3.6 Research and Development

Light detection and ranging (LIDAR)

LIDAR is a remote sensing technique first developed in 1963 [64]. The basic construction of LIDAR is the laser, scanner, photo-detector and navigation system. Examples of instances where LIDAR is used are to map terrains, measure shorelines, measure chemicals in the atmosphere and even in speed cameras. Some studies have shown that LIDAR has been used to detect snow on mars [65]. From this, it can be seen that the applications of LIDAR are extremely versatile. Figure (1.9) shows an image of how LIDAR would map out the surface of a terrain. The variation in colors can be predefined to refer to different values of depth. In this case, green refers to ground level and red the maximum height such as the top of a mountain. The yellow refers to levels existing between the green and red boundaries such as valleys.

LIDAR can be performed from a variety of different platforms namely, the ground, on an aircraft or even a satellite [66]. Depending on the scenario, the basic operation will involve a laser firing a series of pulses (up to 150 000 pulses per second) at the terrain. The scanner and photo-detector work together on detecting and measuring the light being reflected off of the target [66]. The measured data is then analyzed using equation 1.13 to draw a three dimensional map of the surface. If the measurements are taken from the air, any changes in altitude and position are also recoded by the navigation systems and incorporated into the calculations [66]. LIDAR is similar to lunar ranging and SLR, however it uses much more sensitive

photo-detectors which do not rely on retro-reflectors to provide feedback of the surface [66]. Such application is very useful in hostile landscapes or areas which experience severe weather patterns.

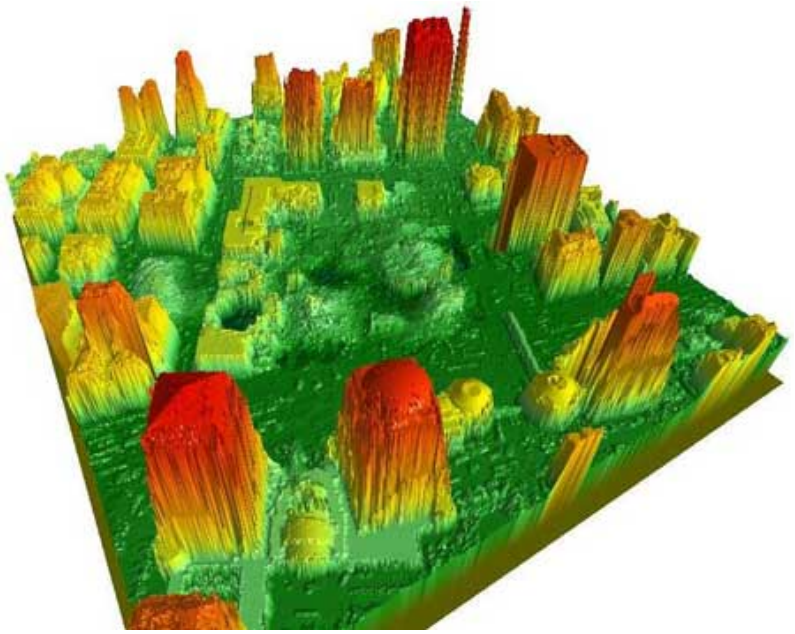

Figure 1.9: LIDAR used in mapping the surface of a terrain [67]

Compact laser systems for displays

The first proposal of using lasers as a display source was in 1960 [68]. At that time, the availability of red, blue and green lasers were limited due to the high cost and large size. In this day, the size of lasers are becoming more and more compact and their availability has increased drastically. The production of compact lasers is now possible using these modern capabilities.

The Ferdinand-Braun-Institute (FBH) are developers of the latest laser technology. One of their most recent developments is the compact laser system used for displays. The application of this product could be for televisions, planetariums and even

flight simulators [69]. FBH improved the conventional system which made use of hybrid micro bench technology. The conventional design used frequency conversion which entailed using an infrared laser of wavelength 976 nm and was converted into blue light by means of a non-linear crystal [69]. This produced more than 1 W of continuous wave blue light at a wavelength of 488 nm. Previously this could only be achieved in a laboratory. FBH has managed to miniaturize the unit to the size of a matchbox (25× 10× 50 mm) [69]. It also provides the ability to be adapted to any wavelength making it extremely versatile.

In the future, many displays will be replaced by laser backlit systems. They will be low cost, less complex and have the ability to be used on any display scale. These traits are very promising since the upside will be display screens which boast extremely high resolutions and brightness capabilities [70, 71].

The vast application of lasers in this day and age is boundless. Therefore new information of their behaviors will always be useful in their respective domains. Developing equipment which can easily and readily measure thermal turbulence is highly sought after since conventional methods use very expensive and bulky equipment and require sophisticated equipment to capture and analyze the data. In light of this, we have developed and have continuously tested the effectiveness of our apparatus which has previously proven to be highly accurate and robust for thermal turbulence detection. This work aims to provide an extension for the use of a PDI in being able to detect thermal as well as directional perturbations in an

in-house developed heated wind tunnel.

1.4 Factors influencing laser beam propagation

Variations in the refractive index of the atmosphere results in atmospheric turbulence. The effects of atmospheric turbulence are often noticeable to a discerning bystander in a number of ways some of which include, wandering (slow oscillatory movement of an image), twinkling (the varying of an images brightness), tremor disk (spreading of the image), dancing (the constant motion of an image about its mean point), quivering (when an image moves away from its initial position), pulsation (when an image changes size) and image distortion (when an image loses focus and become blurry) [72].

These effects typically occur when viewing bright objects in the distance such as lights or a star in the sky. For laser beams, these effects will be difficult to measure or categorize, hence broader aspects are used, namely, beam wander, beam spread, scintillation and spot dancing. Beam wander describes the rapid movement of a laser beam when viewed on a screen some distance away [73]. This movement is attributed to large scale turbulence existing in its propagation path. Beam spreading occurs when the beam unusually spreads in size and does not follow an expected diffraction spread [72]. Scintillation is defined as random changes in a beams intensity [73]. This phenomena occurs mainly through refractive index changes in the atmosphere. Spot dancing is the movement of the beam about its mean central point [74]. The theory behind each of these discussion points have

been expanded upon in section 2.1.

1.5 Basic He-Ne laser design

The helium neon laser is one of the most common and inexpensive lasers in production [3]. Figure (1.12) provides the basic construction of a He-Ne Laser. The collimation of the laser beam is accomplished by the reflectors at each end of the laser. The gas reservoir consists of 85% of helium and 15% neon gas at 1/300 atmospheric pressure.

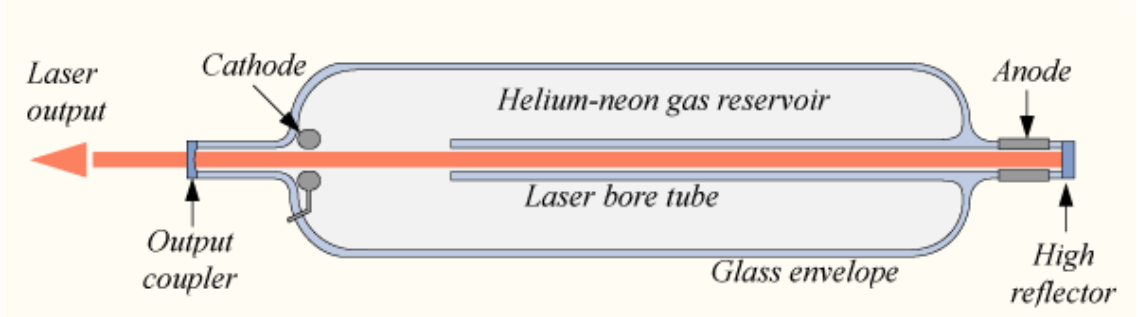

Figure 1.10: Basic He-Ne laser construction [75]

1.6 Properties of lasers

General laser theory states four properties of lasers. Monochromaticity, coherence, direction and brightness [76]. The colour of a laser depends on the type of laser. The electromagnetic wave being amplified is the only frequency existing within the cavity, and hence the only oscillation which can occur at the resonance frequency [76]. For this reason, a laser will always be monochromatic. The next concept is coherence. A laser is regarded as coherent since the process of amplification which takes place within the laser causes all emitted photons to be at the same phase. The outcome

of the photons being "in step" is that at any time their phase difference is constant and at the same frequency [76]. The third property is directionality. The main contributing factor of directionality is in the design of the laser. The parallel mirrors at each end constrain the final beam to a set direction. This ensures that any light which is slightly off axis will be lost from the emerging beam [76]. Lastly, the property of brightness or radiance. Brightness is commonly defined as the power output per unit surface area per unit solid angle. The main contributor of the high level of brightness is the fact that the laser is highly directed. By focusing the beam, the intensity can be made much larger. Even a laser beam of moderate power output has a radiance which is several orders of magnitude larger than that of the most powerful incoherent sources [76]. This trait is highly beneficial in many laser applications.

1.7 Types of lasers

Lasers fall into a wide variety of categories but are often divided by the active material used in the laser such as solid state, liquid state, gas state or free electron [76]. It is also common to refer to lasers by the wavelength of the radiation emitted by the laser such as visible light, infrared, ultra violet (UV) and X-ray lasers. Lasers cover a wide range of power outputs as well. Depending on the application, continuous wave (cw) lasers can start from a few milliwatts (mW) for instance in a laser pointer, to a wide range of kilowatts (kW) for industry such as welding and up to approximately 5 megawatts (MW) for military applications such as directed high energy weapons. The other type of laser is a pulsed laser which can output up to 1

Petawatt of energy. The duration of the output can vary from a few milliseconds to the approximately 1 femtosecond (fs). The actual dimensions of the laser can also be a widely ranging factor. Here again, the application of the laser will determine what size laser should be used. The cavity length can vary from 1 micrometer to up to a few kilometers. In conclusion, lasers can be uniquely customized for the required application and hence it is useful to study their behaviour and establish how they perform in different scenarios. Such knowledge can aid in how we manipulate lasers for different applications and whether or not the outcomes will be successful.

References

[1] Isterling W. M., 2010. *Electro-Optic Propagation Through Highly Aberrant Media*, Phd Thesis, University of Adelaide, Australia.

[2] Adapted from Meteorology for Scientists and Engineers, A Technical Companion Book to C. Donald Ahrens Meteorology Today, 2nd Ed., by Stull, p. 67.

[3] Andrews L. C. & Phillips, R. L., 2005. *Laser Beam Propagation Through Random Media*, SPIE Press, USA.

[4] Murty S.S.R. & Bilbro J.W., 1978. *Atmospheric effects on CO2 laser propagation.*

[5] McDonough J., 2007. "LECTURES on TURBULENCE", University of Kentucky.

[6] Gibson C., 1991. *Kolmogorov similarity hypotheses for scalar fields: sampling intermittent turbulent mixing in the ocean and galaxy*, In

Proceedings of the Royal Society of London A: Mathematical, Physical and Engineering Sciences, Vol. 434, 1890, 149-164.

[7] Maronga, B., Moene, A., van Dinther, D., Raasch, S., Bosveld, F. & Gioli, B., 2013. *Derivation of structure parameters of temperature and humidity in the convective boundary layer from large-eddy simulations and implications for the interpretation of scintillometer observations*, Boundary-Layer Meteorology, 148(1), 1-30.

[8] Weichel H., 1990. *Laser Beam Propagation in the Atmosphere*, SPIE, USA.

[9] Magee E. P., 1993. *Characterisation of Laboratory Generated Turbulence*, MSc Thesis, Air Force Institute of Technology, United States.

[10] Strohbehm J. W., 1978. "Laser Beam Propagation In The Atmosphere", New York, Springer-Verlag.

[11] Gamo H. & Majumdar A.K., (1978). "Atmospheric turbulence chamber for transmission experiment: characterisation by thermal method," *Appl. Opt.*, 17, 3755-3762.

[12] Gochelashvili K., (1971). "Saturation of the Fluctuations of Focused Radiation in a Turbulent Medium," *Radiophys. Quant. Electron*, 14, 470-473.

[13] Ngo Nyobe E., Pemha E., Hona J., Bilong II J. and Lamara M., *Measurement of the structure coefficient of refractive index fluctuations in a*

turbulent premixed butane-air flame by means of a laser-based interferometer technique, Optics and Lasers in Engineering, **59**, 41-49 (2014).

[14] Murty S.S.R. & Bilbro J.W., 1978. *Atmospheric effects on CO_2 laser propagation.*

[15] Barrett J.L. & Budni P.A., 1992. *Laser beam propagation through strong turbulence*, Journal of Applied Physics, 77(3), 1124-1127.

[16] Hogge C. B. & Visinsky W. L. *Laser beam probing of jet exhaust turbulence*, Applied optics, 10.4, 889-892 (1974).

[17] Gilbert K. G., Hogge C. B. & Visinsky W. L., 1970. *Laser Beam Propagation through Jet Exhaust,* Air Force Weapons Laboratory TR-70-128.

[18] Tatarski V. I., 1961. *Wave Propagation in a Turbulent Medium*, McGraw-Hill, New York.

[19] Kerr J. R., *Multiwavelength Laser Propagation Study-II,* Quart. Progr. Rep. No. 3, Oregon Graduate Center for Study and Research, Portland, Ore.

[20] Wright N. J. & Schultz R. J., 1967. *Measurement of the Refractive Index Structure Coefficient-C*, BRL Memor. Rep. 1885.

[21] Isterling W.M., Cox L.J., Dubovinsky M., Titterton D.H. & Porter T., 2005. *Laser Interaction with Jet Engine Exhaust Induced Turbulence*, Laser, 7, p.9.

[22] Brown W., (1972). "Moment Equations for Waves Propagated in Random Media", *J. Opt. Soc. Am.*, 62, 45-54.

[23] Brown W., (1972). "Fourth Moment of a Waves Propagating in a Random Media", *J. Opt. Soc. Am.*, 62, 966-971.

[24] Brown W., (1972). "Moment Equations for Waves Propagated in Random Media", *J. Opt. Soc. Am.*, 62, 45-54.

[25] deWolf D., (1973). "Strong Irradiance Fluctuations in Turbulent Air, Part 1: Plane Waves," *J. Opt. Soc. Am.*, 63, 171-179.

[26] deWolf D., (1973). "Strong Irradiance Fluctuations in Turbulent Air, Part 2: Spherical Waves," *J. Opt. Soc. Am.*, 63, 1249-1253.

[27] deWolf D., (1974). "Strong Irradiance Fluctuations in Turbulent Air, Part 3: Diffraction Cutoff," *J. Opt. Soc. Am.*, 64, 360-365.

[28] Bufton J.L., Minott P.O., Fitzmaurice M.W., Titterton P.J., *Measurements of turbulence profiles in the troposphere*, Journal of the Optical Society of America, **62**, 9, 11171120 (1972).

[29] Coulman C.E., 1973. *Vertical profiles of small-scale temperature structure in the atmosphere*, Bound.-Layer Meteor., **4**, 169177.

[30] Obukhov A. M., 1941. *On the Distribution of Energy in the Spectrum of Turbulent Flow,* Doklady Akad, Nauk SSSR, 32 (4), 19.

[31] Kolmogorov A. N., 1941. *Dissipation of Energy in Locally Isotropic Turbulence,* Doklady Akad, Nauk SSSR, 32.

[32] Bufton J.L., 1975. *A radiosonde thermal sensor technique for measurement of atmospheric turbulence.*

[33] Warnock J. M. & VanZandt T. E., *A statistical model to estimate the refractivity turbulence structure constant C_n^2 in the free atmosphere*, NOOA Tech. Memo ERL, AL-10, Aeronom. Lab., Boulder, CO, (1985).

[34] Augustine S. M. & Chetty N., 2014, *Experimental verification of the turbulent effects on laser beam propagation in space*, Atmósfera, 27(4), 385-401.

[35] Ndlovu S. C. & Chetty N., 2015, *Experimental determination of thermal turbulence effects on a propagating laser beam*, Open Physics, 13(1).

[36] Carnevale, M., *et al.*, (2013). *Uncertainty quantification: A stochastic method for heat transfer prediction using LES*, Journal of Turbomachinery **135**, 5.

[37] Carnevale, Mauro, *et al.*, (2014). *Film Cooling and Shock Interaction: An Uncertainty Quantification Analysis With Transonic Flows*, ASME Turbo Expo 2014: Turbine Technical Conference and Exposition. American Society of Mechanical Engineers.

[38] Covington H., 1996. *Model designation of military aerospace vehicles*, (No. DOD-4120.15-L). OFFICE OF THE UNDER SECRETARY OF DEFENSE (ACQUISITION AND TECHNOLOGY) WASHINGT ON DC.

[39] http://cdn.phys.org/newman/gfx/news/hires/uav.jpg viewed 20 February 2016.

[40] *Defense IQ talks to Dr Paisek about Directed Energy Weapon systems*, 2012. Defence iQ'.

[41] Spectrum Tutorial, University of Wisconsin Electromagnetic Spectrum Tutorial viewed 22 June 2013.

[42] US lasers? PLA preparing to raise its deflector shields - SCMP.com, viewed on 12 April 2015.

[43] Ezekiel S. & Balsamo S.R., 1977. *Passive ring resonator laser gyroscope.* Applied Physics Letters, 30(9), 478-480.

[44] Takase K., 2008. *Precision rotation rate measurements with a mobile atom interferometer*, Doctoral dissertation, Stanford University.

[45] http://laserfest.org/lasers/images/inn-gyroscope.gif viewed 14 March 2016.

[46] Alastair D. M., 2011. *Military Laser Technology for Defense: Technology for Revolutionizing 21st Century Warfare*, John Wiley & Sons.

[47] http://laserfest.org/lasers/images/inn-designation.jpg viewed 03 March 2016.

[48] Basting D., Pippert K.D. & Stamm U., 2002. *History and future prospects of excimer lasers*, In Second International Symposium on Laser Precision Micromachining, 25-34.

[49] Hicks R., 2009. *Understanding Cancer*, Second Ed., Southwood Press Pty Ltd., Brisbane.

[50] Lonappen A., Bindu G., Thomas V., Jacob J., Rajasekaran C. and Mathew K. T., 2007. "Diagnosis of Diabetes Mellitus Using Microwaves", *Journal of Electromagnetic Waves and Applications*, 21, 10.

[51] Ibrahim A. T., 2007. "Using Microwave Energy To Treat Tumors", *Progress In Electromagnetic Research B*, 3, .1-27.

[52] Chang A.W., Tsang A.C., Contreras J.E., Huynh P.D., Calvano C.J., Crnic-Rein T.C. & Thall E.H., 2003. *Corneal tissue ablation depth and the Munnerlyn formula*, Journal of Cataract & Refractive Surgery, 29(6), 1204-1210.

[53] http://laserfest.org/lasers/images/inn-eye.jpg viewed 12 October 2016.

[54] Huang D., Swanson E.A., Lin C.P., Schuman J.S., Stinson W.G., Chang W., Hee M.R., Flotte T., Gregory K., Puliafito C.A. & Fujimoto J.G., 1991. *Optical coherence tomography*, Science (New York, NY), 254(5035), 1178.

[55] Liang X., Crecea V. & Boppart S.A., 2010. *Dynamic optical coherence elastography: a review*, Journal of innovative optical health sciences, 3(04), 221-233.

[56] Ojo J. S., Ajewole M. O. and Sarkar S. K., 2007. "Rain rate and rain attenuation prediction for satellite communication in Ku and Ka bands over Nigeria", *Progress In Electrodynamics Research B*, 5, 207-223.

[57] Tapley B.D., Schutz B.E. & Eanes R.J., 1986. *Satellite laser ranging and its applications*. In Fundamental Astronomy and Solar System Dynamics, 247-261.

[58] Lubin P. & Hughes G.B., 2015. *Directed Energy for Planetary Defense*, Handbook of Cosmic Hazards and Planetary Defense, 941-991.

[59] http://chem.lapeer.org/PhysicsDocs/Goals2000/Laser1.html viewed 27 September 2016.

[60] http://laserfest.org/lasers/images/inn-cutting.jpg viewed 17 March 2016.

[61] Jha D.G., 2013. *Computer Concepts and Management Information Systems*, PHI Learning Pvt. Ltd.

[62] https://upload.wikimedia.org/wikipedia/commons/b/b4/Classical_spectacular_laser_effects.jpg viewed 14 March 2016.

[63] *Laser perimeter intrusion detection system*, U.S. Patent 3,623,057, issued November 23, 1971.

[64] Sharma A., Sivakumar V., Bollig C., Van der Westhuizen C. & Moema, D., 2009. *System description of the mobile LIDAR of the CSIR*, South Africa. South African Journal of Science, 105(11-12), 456-462.

[65] Neumann G.A., Smith D.E. & Zuber M.T., 2003. *Two Mars years of clouds detected by the Mars Orbiter Laser Altimeter*, Journal of Geophysical Research: Planets, 108(E4).

[66] Tao C.V. & Li J. eds., 2007. *Advances in mobile mapping technology*, Vol. 4., CRC Press.

[67] http://laserfest.org/lasers/images/inn-lidar.jpg viewed 04 July 2016.

[68] Korpel A., Adler R., Desmares P. & Watson W., (1966). *A television display using acoustic deflection and modulation of coherent light,* Appl. Opt. 5, 16671675.

[69] http://www.photonics.com/Article.aspx?AID=41519 viewed 12 September 2016.

[70] Chellappan K.V., Erden E. & Urey H., 2010. *Laser-based displays: a review*, Applied optics, 49(25), F79-F98.

[71] Janssens P. & Malfait K., 2009. *Future prospects of high-end laser projectors*, In SPIE OPTO: Integrated Optoelectronic Devices, pp. 72320Y-72320Y.

[72] Quirrenbach, A., 2006. *The effects of atmospheric turbulence on astronomical observations*, A. Extrasolar planets. Saas-Fee Advanced Course 31, 137, 137.

[73] Berman G.P., Gorshkov V.N. & Torous, S.V., 2011. *Scintillation reduction for laser beams propagating through turbulent atmosphere*, Journal of Physics B: Atomic, Molecular and Optical Physics, 44(5), p.055402.

[74] Chiba T., 1971. *Spot dancing of the laser beam propagated through the turbulent atmosphere*, Applied optics, 10(11), 2456-2461.

[75] https://upload.wikimedia.org/wikipedia/commons/a/af/Hene-1.png viewed 14 July 2016.

[76] Svelto O., 2010. *Principles of Lasers*, Springer US, 9-15.

Chapter 2

THEORY

In Chapter 1, we classified the atmosphere and the eddies which exist as a result of temperature variations existing between the thermal layers. The optical effects experienced by a laser beam are due to the interactions of the beam with any refractive index variations along its path. It has been found that the temperature fluctuations can be defined by the same spectral laws which are used to classify velocity fluctuations [1, 2]. The velocity spectrum defines the energy of the eddies and it is commonly denoted by $\phi(\overline{K})$ where $\overline{K}$ is the wavenumber and is equal to $\frac{2\pi}{l}$ where l represents the size of the eddy [3].

Kolmogorov's theory of turbulence assumes that the atmosphere is homogeneous, isotropic and independent from large scale turbulence [3]. In addition, Kolmogorov assumed that energy enters a system at a rate ϵ per unit mass and generates large scale turbulence also known as the outer scale of turbulence L_0. The rate of

dissipation can be determined through [1],

$$\epsilon_0 = 2\nu \int_0^\infty k^2 E(k) dk. \tag{2.1}$$

In the work of Lioa and Su [4] Kolmogorov's theory was validated through experimentation. In their work, direct numerical simulations of turbulence were performed and compared to Kolmogorov's existing results. These results showed very close approximation to each other, proving that Kolmogorov's theory developed in 1941 [5] is still valid using advanced numerical simulations in 2015 [4]. We have adopted the Kolmogorov theory into our work since we have assumed the same hypothesis. More specifically we assume that turbulence does not exceed the outer scale L_0 and does not fall below the inner scale l_0 i.e. $(L_0 < l < l_0)$ [1]. This range is known as the inertial sub-range and can be extended to a larger scale by setting limits of $l_0 \rightarrow 0$ and $L_0 \rightarrow 0$.

In the works of Reynolds [6], two types of flow were identified, namely laminar and turbulent. A graphical view of the two flows is depicted in Figure (2.1), Laminar flows are organised, slow, and parallel where as turbulent flows consist of high speed velocities, random displacements and are disorganised. Reynolds developed a dimensionless value to represent flow, namely [7],

$$R_e = \frac{u\,L}{\nu}, \tag{2.2}$$

where, u is the mean velocity, ν is the kinematic viscosity of the fluid and L,

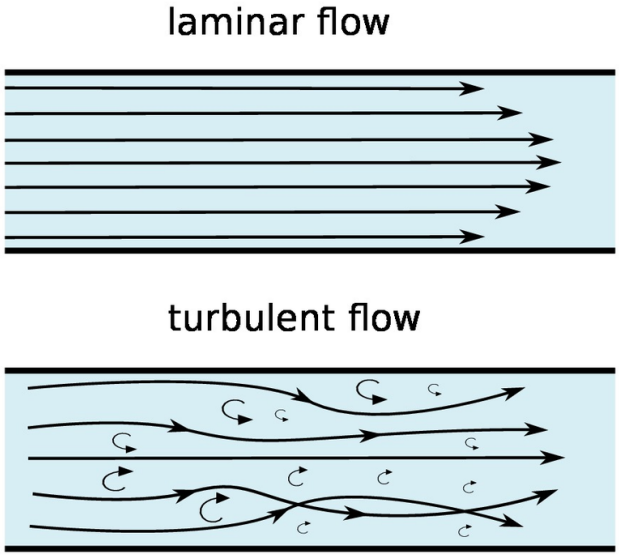

Figure 2.1: Laminar and turbulent flow

the path length. For laminar flow, R_e<2300 and for turbulent flow, R_e>4000. Typically, the atmosphere is regarded as having a highly turbulent flow with R_e=10^5.

The Kolmogorov theory also states a $\overline{K}^{-11/3}$ dependence for the 3 dimensional wavenumber up to a maximum value of $\overline{K}_m$. $\overline{K}_m$ is related to the inner scale of turbulence through [7],

$$\overline{K}_m = \frac{5.92}{l_0}. \tag{2.3}$$

The outer scale of turbulence is related to $\overline{K}_m$ by [7],

$$\overline{K}_0 = \frac{2\pi}{L_0}. \tag{2.4}$$

As the spatial wavenumber increases beyond $\overline{K}_0$, turbulence tends toward being more isotropic and homogeneous. In general, the refractive index n can be related

to the wavelength of the laser through the relation [7],

$$n = \frac{77.6\,P}{T}\left[1 + \frac{0.00753}{\lambda^2} \times 10^{-6}\right] \tag{2.5}$$

where all variables have their usual meanings. C_n^2 can also be derived through the refractive index by [7],

$$C_n^2 = \frac{\langle (n_2 - n_1)^2 \rangle}{r^{2/3}}, \tag{2.6}$$

where n_2 and n_1 represent the refractive indexes at 2 points separated by a distance r.

Tartarski [8] has described the general form for the refractive index spectrum under the assumption that the temperature spectrum and the refractive spectrum are the same as the velocity spectrum,

$$\phi_n(\overline{K}) = 0.033\,C_n^2\,K^{-11/3}\,e^{\frac{-\overline{K}^2}{\overline{K}_m^2}} \tag{2.7}$$

For the instance of $\overline{K}$=0, the refractive index describes a singularity. Tartarski [8] defines this implication as the energy per unit volume which becomes unbounded in proportion to the eddy size. To counteract this scenario, the modified von Karman spectrum is incorporated and yields the expression [8],

$$\phi_n(\overline{K}) = \frac{0.033\,C_n^2 \exp\left[-\overline{K}^2\left(\frac{l_0}{2\pi}\right)^2\right]}{\left[\overline{K}^2 + \left(\frac{L_0}{2\pi}\right)^2\right]^{11/6}} \tag{2.8}$$

These models fail when turbulence is not homogeneous. Figure (2.2) presents a graph which shows a comparison between the Tartarski, modified von Karman and

Kolmogorov's spectrum.

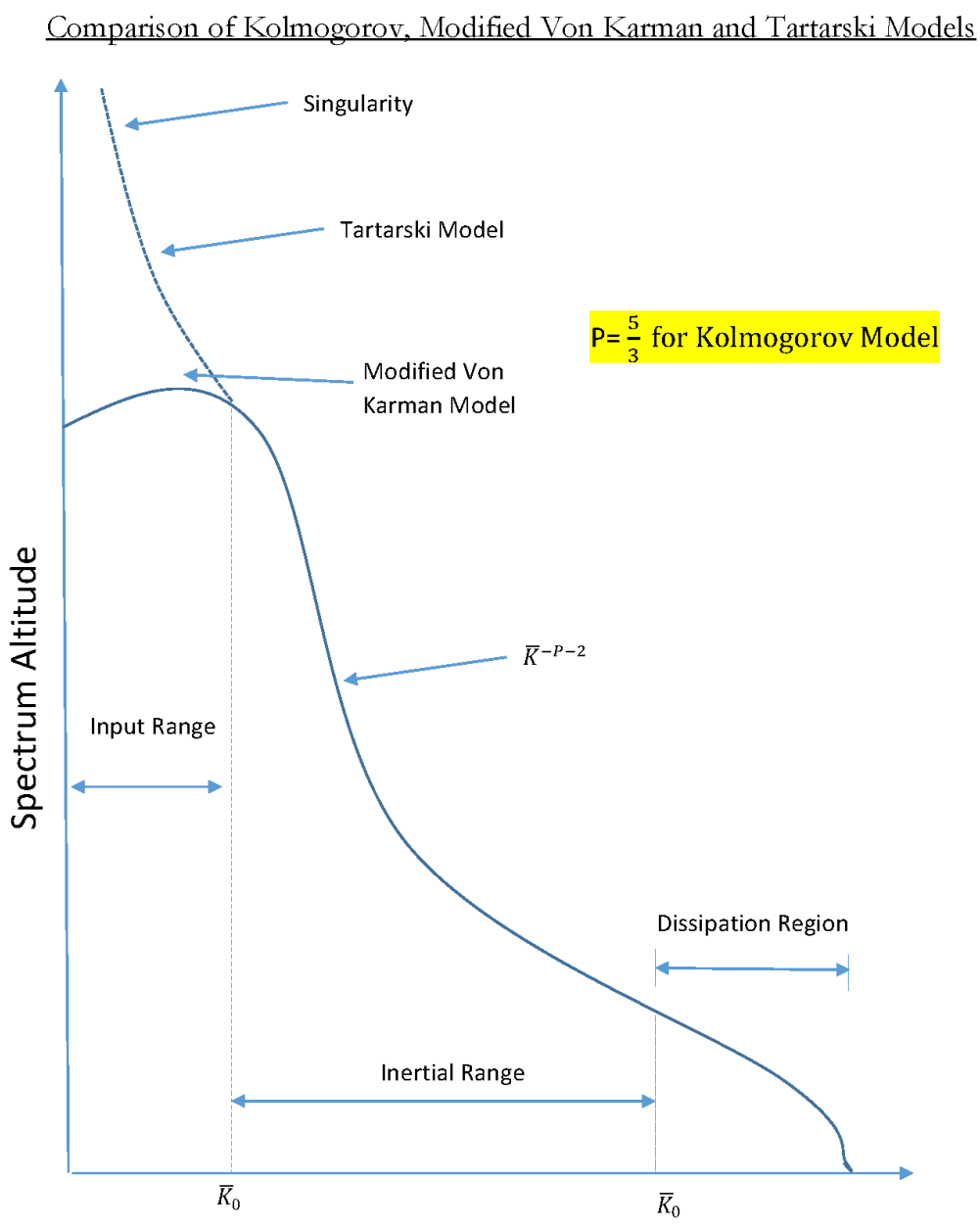

Figure 2.2: Comparison of models for the refractive index fluctuations [3]

It can be shown from equation 1.4 that the size of the eddy determines the severity of the refractive index structure function. This relation can be generalised through [8],

$$\left\langle \left(\delta_n(l)\right)^2 \right\rangle = C_n^2\, l^{2/3}. \tag{2.9}$$

where l is the diameter of the eddy.

In summary, a broad generalisation can be made in terms of how the atmosphere can be viewed. Since each eddy causes refraction on various scales, we can consider the atmosphere to be full of lenses of different sizes and focal points. In this way, the theory of lenses can be applied to determine the outcomes of incoming light.

2.1 Effect of turbulence on laser beams

The He-Ne laser used in this work has a Gaussian wave profile and the characteristics of being stable, coherent and directed [9]. By propagating the laser beam through various inhomogeneities, the wave form becomes perturbed [9]. These inhomogeneities arise from the interaction of turbulent causing sources with the atmosphere which leads to random fluctuations of the atmosphere [9, 10]. These inconsistencies in the atmosphere interact with the wave form of the laser beam, causing the light to bend, change direction and lose coherence [11]. Characteristics of a Gaussian beam can be measured through the beam radius w(z) and the radius

of the curvature of the phase front R(z) [12],

$$\mathrm{w(z)} = \mathrm{w_0}\sqrt{1 + \left(\frac{\lambda \mathrm{z}}{\pi \mathrm{w_0^2}}\right)} \tag{2.10}$$

and

$$\mathrm{R(z)} = \mathrm{z}\left(1 + \frac{\pi \mathrm{w_0^2}}{\lambda \mathrm{z}}\right)^2, \tag{2.11}$$

where,

- $\mathrm{w_0}$ represents the radius of the beam at its waist and
- λ represents the wavelength of the laser beam.

Without any applied turbulence, we can expect the beam to have a far field angular spread according to the ratio $\theta = \frac{2\,\lambda}{\pi\, d}$ [12]. Once turbulence is applied along the laser beams path, temporal and spatial effects will be experienced in the direction and phase of the wavefront [3]. This in turn leads to larger scattering by the turbulent eddies and causes greater spreading. Eddies which are larger than the beam diameter will cause deflection of the beam [3]. In other words, the beam will deflect away from the its initial straight line path. For eddies which are smaller than the beam diameter, portions of the beam are diffracted which causes the phase front to become corrugated. The implication of this is constructive and destructive interference in the form of bright and dark fringes. These effects can broadly be captured as scintillation of the beam. Since turbulence consists of various types of inhomogeneities, a laser beam can experience any of the previously mentioned effects such as beam wander and spread. Key characteristics such as the path length, source of turbulence, strength of turbulence, laser power and laser

wavelength also play important roles in the severities of the effects.

During simulations, we often have to compensate for the previously mentioned effects. Such enhancements come in the form of neutral density filters, spatial filters and collimators. With these enhancements, the laser beam can be directed and focused onto the target with minimal amounts of stray light artifacts being present [3]. The angle of divergence can be measured according to the equation [9],

$$\theta = \frac{\mathrm{w(z)}}{\mathrm{z}} \tag{2.12}$$

$$= \frac{\lambda}{\pi \mathrm{w}_0} \qquad \text{for z} \gg \mathrm{Z}_R = \frac{\pi w_0^2}{\lambda}, \tag{2.13}$$

where Z_R is known as the Rayleigh range.

2.1.1 Scintillation

Turbulent eddies cause fluctuations in the refractive index of the atmosphere which cause diffractive scattering of light in the laser beam. This phenomena is known as scintillation. Large eddies act as lenses and can cause the laser light to either focus or defocus while smaller eddies cause a scattering effect. The actual size of the eddies depends on the Fresnel zone [3]. The smallest eddies are smaller than the first Fresnel zone defined by $\sqrt{L/k}$ where [13],

- L is the path length and
- k is the wavenumber

The scintillation variance can be measured through,

$$\sigma_r^2 \;=\; k^{7/6}\sec^{11/6}\theta \int_0^\infty dh\, h^{5/6} C_n^2(h), \tag{2.14}$$

where,

- θ is the zenith angle
- h is the height of the receiver above ground level.

A graphical description of turbulent eddies is provided in Figure (2.3). The largest eddies contain the most amount of energy and break down through the process of energy dissipation. The result of this process leads to multiple smaller, more stable eddies.

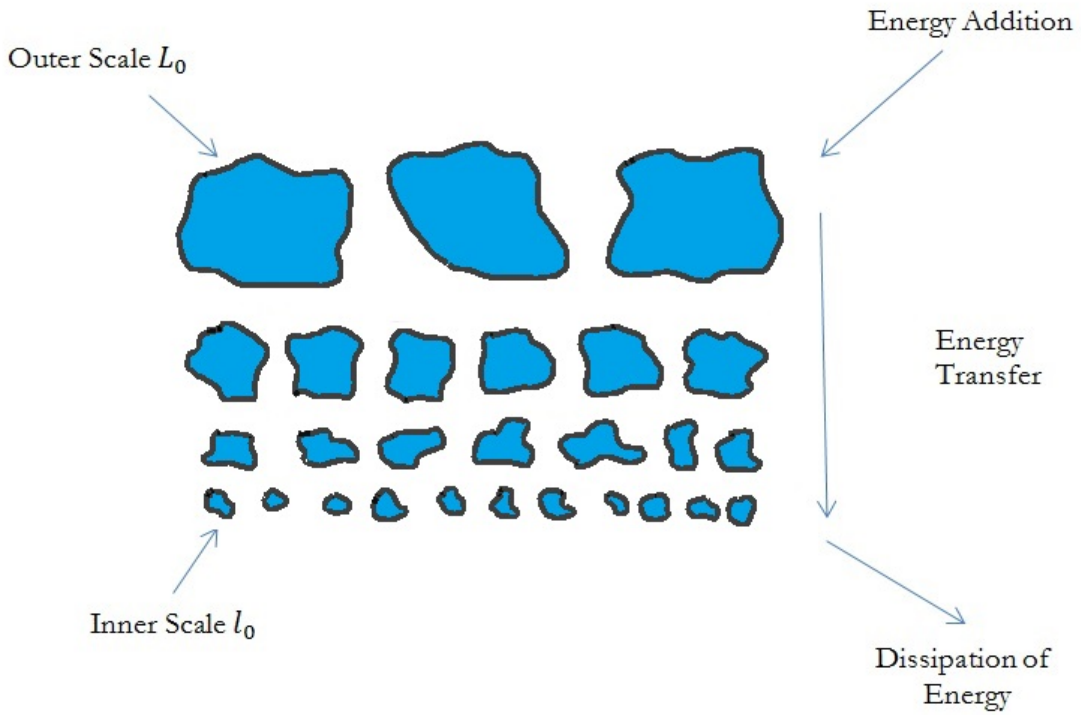

Figure 2.3: Turbulent eddies

2.1.2 Spot Size

The rate of diversion is determined by the beam radius (or spot size) [3]. The spot size varies as the laser beam propagates through a turbulent medium. Banish *et al.* states that the greatest influence on spot size results from turbulent cells sizes which are greater than the wavelength of the light and less that the beam diameter. A small spot size diverges quicker and over short distances whereas a large spot size diverges slower and over longer distances. Only the beam radius increases during propagation according to [10, 14, 15],

$$\mathrm{w(z)} = \mathrm{w_0}\sqrt{1 + \left(\frac{\lambda \mathrm{z}}{\pi \mathrm{w_0^2}}\right)}, \tag{2.15}$$

where $w(z)$ represents the spot size and all other variables have their usual meanings

2.1.3 Beam Wander

The implication of beam wander on a laser is a beam which deviates on and off its initial straight line course. These deviations are caused by a varying refractive index due to turbulent eddies. Characterisation of beam wander can be calculated statistically through the variance of the angular displacement [16–18],

$$\sigma_d^2 = 2.92\, D^{-1/3} \int_0^L dz\, C_n^2(z) \frac{\left(1 - \frac{z}{L}\right)^2}{\left|1 - \frac{z}{F}\right|^{1/3}}, \tag{2.16}$$

where,

- D is the diameter of the initial beam,

- z is position along the path,
- L is the propagation path length and
- F is the geometric focal range of the initial beam.

2.1.4 Beam Spreading

Beam spreading is the widening of the beam as it propagates through the atmosphere [19]. Two main types of beam spreading occur, long and short term. Short term describes the spreading of the beam at an instant in time. Long term beam spread describes the beam spread over long time averages [15]. The difference between beam wander and beam spread is the size of the turbulent eddies which interact with the laser beam [19]. For beam wander, the turbulent eddies are larger than the beam whereas in beam spread the turbulent eddies are much smaller than the beam. The most apparent implication of beam spread is a redistribution of energy of the laser beam. Figure (2.2) provides an example of how beam spread can be interpreted graphically.

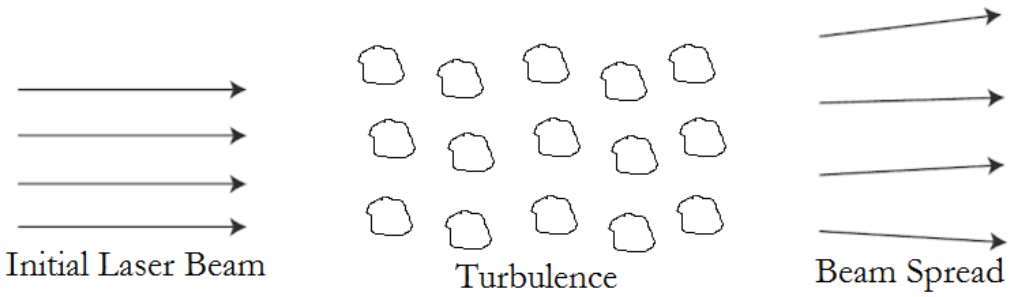

Figure 2.4: Example of beam spread

2.1.5 Rytov Theory

The Rytov approximation (σ_R^2) provides a qualitative description of all the statistical properties using simple equations for describing the wave field. The basic assumptions for the approximation to apply are l_0=0, L_0=∞ and constant C_n^2 along the path length. According to [20],

$$\sigma_R^2 = \frac{\langle I^2 \rangle}{\langle I \rangle} - 1 \tag{2.17}$$

$$= 1.23\, C_n^2\, k^{7/6}\, L^{11/6} \tag{2.18}$$

where I is the signal irradiance, k and L have their usual meanings. The averaged ensemble implies that the approximation is a variance of intensity fluctuations. In general, the Rytov approximation is used to distinguish between weak and strong turbulence. For strong turbulence, σ_R^2>>1, for moderate turbulence σ_R^2=1 and for weak turbulence σ_R^2<<0 [20].

Equation 2.17 represents the Rytov variance for a plane wave and has been found to inadequately describe a Gaussian wave since weak scintillation describes the entire beam profile being less than 1. Work by Thomas F. [21] has generalised laser beam propagation according to three models: the first being an infinite plane wave, then second in a spherical wave and third by the Gaussian wave. We have established that the laser used in this work has a Gaussian beam profile and hence we will discuss the Rytov theory particularly for this scenario.

The field of the Gaussian beam as it traverses the propagation path z can be determined by [21],

$$U(r,z) = \frac{1}{4\,\pi\,z}\exp\left[i\,k\,z + \frac{i\,k\,r^2}{2\,z}\right], \tag{2.19}$$

where, r is the perpendicular distance to z, $i = \sqrt{-1}$ and k the wavelength. From the three models, the Gaussian beam wave has shown to be the most accurate since it is finite and has a constant amplitude. The lowest order field can be determined at z=0 as [21],

$$U(r,0) = a_0 \exp\left[-\frac{r^2}{W_0^2} - i\frac{k\,r^2}{2\,F_0}\right], \tag{2.20}$$

where, a_0 represents the constant amplitude, F_0 is the radius of the phase front and W_0 the radius of the Gaussian beam at the transmitter [21].

To determine the field at the receiver, a generalised formula can be used, [21],

$$\begin{aligned} I(r,L) &= \frac{1}{\Theta_0^2 + \Lambda_0^2}\exp\left(-\frac{2\,r^2}{W^2}\right), & (2.21)\\ &= \left(\Theta_0^2 + \Lambda_0^2\right)\exp\left(-\frac{2\,r^2}{W^2}\right), & (2.22) \end{aligned}$$

when Θ and Λ are zero, the Gaussian model represents a plane wave. When $\Theta = 1$ and $\Lambda = 0$, the Gaussian wave represents a spherical wave. In this way, the mean intensity at the receiver can be determined for any of the models.

2.2 Effects of aerosols on laser beams

Aerosols in the atmosphere can exist through a variety of sources [24]. Steam, fog, vehicle exhaust fumes, haze, dust and smoke are examples of both artificial and natural aerosols [24]. The interaction of aerosols with a laser beam is one that becomes scattered and depends on the size and quantity of the particulate in the air. In general, the size of the particulate remains unchanged relative to altitude, however the quantity decreases rapidly with an increase in altitude. Lasers propagating through aerosols lose a significant amount of energy due to a phenomena known as backscatter [3]. The distribution of scatterers can be calculated by,

$$\sigma_0 = 4\,\pi\,\beta\left(\frac{c\tau}{2}\right) \tag{2.23}$$

where,

- c is the speed of light and
- β represents the backscatter coefficient.

Figure (2.4) provides a diagrammatic description of the sources of aerosols and how they cycle within the ecosystem, transferring from one source to the other.

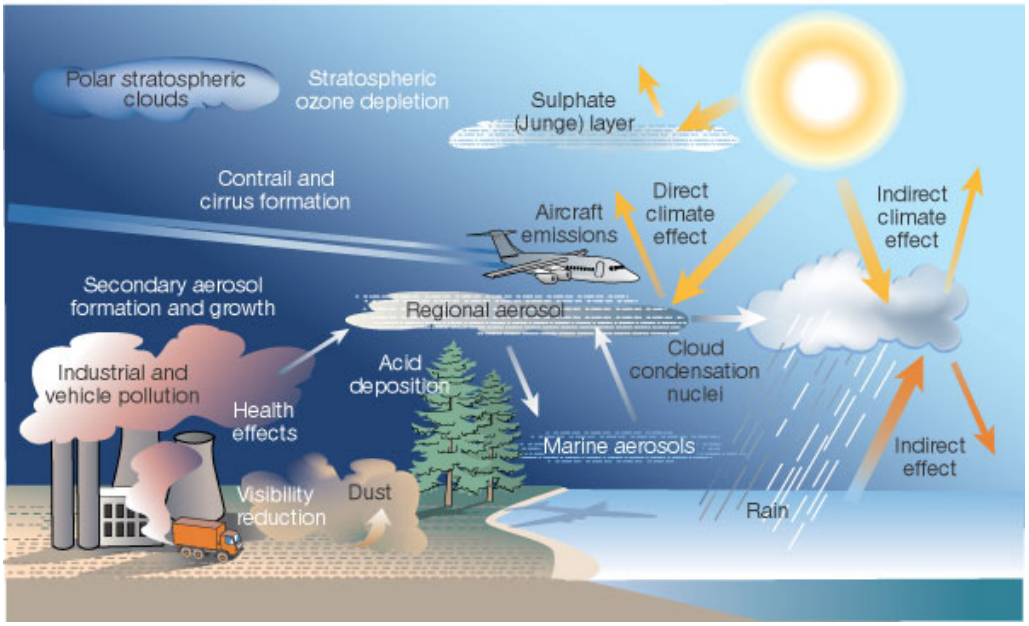

Figure 2.5: Aerosols and their sources [22]

2.3 Interferometry

Interferometers are precise measuring instruments used to measure variations in refractive index, small displacements or surface inaccuracies [23]. The basic idea of the process of measurement begins with a light source propagating through the interferometer. On passing through the interferometer, the beam is split in half by a beam splitter. Half the beam passes straight through and the other is reflected back. The reflected beam, known as the reference beam, thereafter shines onto a mirror and is captured by a camera or screen. The other half of the beam propagates through the medium under consideration and subsequently onto a second mirror. It then propagates back onto the beam splitter and finally onto the camera or screen. The second beam travels a larger distance than the first which results in the two beams being out of phase [23]. The combination of the two beams at the camera or screen produce an interferogram which consists

of light and dark fringes. Light fringes reflect constructive interference and dark fringes indicate destructive interference. Inspection of the interferogram can provide useful information such as how a beam behaves under different perturbing scenarios.

Numerous interferometers exist at present, each deigned and implemented in different ways. In this work, we have used a point diffraction interferometer (PDI) which has proven to be a highly accurate and robust device in detecting both thermal turbulence and directional fluctuations of a laser beam. The PDI employs the same basic operation technique as other interferometers, however the advantage is the common path design which allows for extremely stable interferograms to be produced. In addition, the PDI is cost efficient, robust, easily alignable and small in size. This makes for a useful device when working in the field and capturing data quickly and efficiently.

2.4 Point diffraction interferometer

The first PDI was designed in 1933 by Linnik [25] and later improved by Smartt and Steel [26] in 1975. Figure(2.6) is a depiction of the PDI used in this work. It was designed by Astro Electronics. The full theory of the PDI has previously been defined and discussed in [27] and hence will not be described further. Figure (2.5) is the actual image of the PDI used in this work.

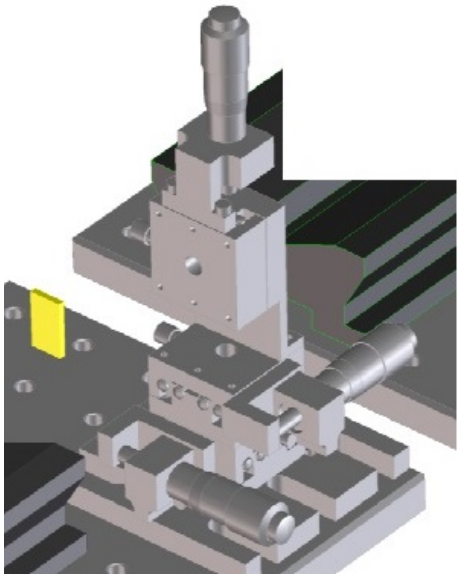

Figure 2.6: PDI

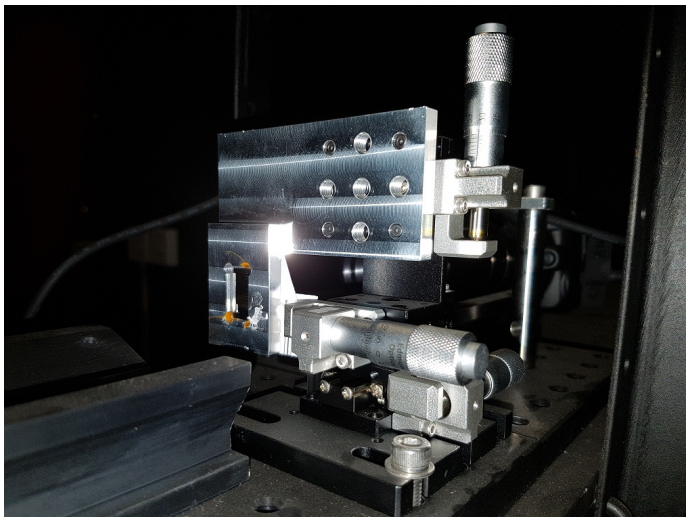

Figure 2.7: Image of the actual PDI

A complete analysis and discussion of the experimental equipment has previously been discussed in [27]. Other tools can be used to measure the signal from the laser beam such as an oscilloscope. However, a PDI is a much more cost efficient option and quick in its implementation. An oscilloscope for instance would require a power source which would be difficult to use in the field.

References

[1] Katul G. & Parlange M., 1994. *On the active role of temperature in surface-layer turbulence*, Journal of the atmospheric sciences, 51(15), 2181-2195.

[2] Quirrenbach, A., 2006. *The effects of atmospheric turbulence on astronomical observations*, A. Extrasolar planets. Saas-Fee Advanced Course 31, 137, 137.

[3] Murty S.S.R. & Bilbro J.W., 1978. *Atmospheric effects on CO_2 laser propagation.*

[4] Liao Z.J. & Su W.D., 2015. *Kolmogorovs hypotheses and global energy spectrum of turbulence*, Physics of Fluids (1994-present), 27(4), p.041701.

[5] Kolmogorov A.N., 1941. *Dissipation of energy in locally isotropic turbulence.* In Dokl. Akad. Nauk SSSR. **32.1**, 16-18.

[6] Jackson D. & Launder B., 2007. *Osborne Reynolds and the publication of his papers on turbulent flow*, Annu. Rev. Fluid Mech., 39, 19-35.

[7] Murty S.S.R., 1976. *Laser Doppler systems in atmospheric turbulence.*

[8] Tatarski V. I., 1961. *Wave Propagation in a Turbulent Medium*, McGraw-Hill Company, New York.

[9] Weichel H., 1990. *Laser Beam Propagation in the Atmosphere*, SPIE, USA.

[10] Andrews L. C. & Phillips, R. L., 2005. *Laser Beam Propagation Through Random Media*, SPIE Press, USA.

[11] Roddier F., 1981. "The effects of atmospheric turbulence in optical astronomy", *In: Progress in optics. Volume 19. Amsterdam, North-Holland Publishing Co. 1981, p. 281-376., 19,* 281-376.

[12] Bass M. & Optical Society of America, 1995. *Handbook of Optics: Fundamentals, techniques, and design*, McGraw-Hill.

[13] Lawrence R. S. & Strohbehn J. W., 1970. "A Survey of Clear-air Propagation Effects Relevant to Optical Communications, *Proc . IEEE*, **58**, 1523 1545.

[14] Webb H. R., 1996. "Confocal optical microscopy", *Reports on Progress in Physics*, 59(3), 427.

[15] Isterling W. M., 2010. *Electro-Optic Propagation Through Highly Aberrant Media*, Phd Thesis, University of Adelaide, Australia.

[16] Ferraro P., Paturzo M. & Grilli S., 2007. "Optical Wavefront Measurement Using a Novel Phase-Shifting Point-Diffraction Interferometer",

[17] Chin S. L., 1989. *Fundamentals of Laser Optoelectronics*, World Scientific Publishing Co. Pte. Ltd., Singapore.

[18] Sasiela R. J., 1989. *Electromagnetic Wave Propagation in Turbulence*, 2nd Edition, SPIE, Washington.

[19] Berman G. P., Chumak A. A. & Gorshkov V. N., 2013. *Beam Wandering in the Atmosphere: The Effect of Partial Coherence*, Los Alamos National

[20] Mohammed, H., & Sadeq A., *Influence of Atmospheric Turbulence on Laser Range Evaluations.*

[21] Thomas F.E., 2005. *The Scintillation Index In Moderate To Strong Turbulence For The Gaussian Beam Wave Along A Slant Path*, Doctoral dissertation, University of Central Florida Orlando, Florida.

[22] https://www.alternative-learning.org/nl/wordpress/?p=13564 viewed 20 February 2016.

[23] Renkens M.J. & Schellekens P.H., 1993. *An Accurate Interference Refractometer Based on a Permanent Vacuum ChamberDevelopment and Results*, CIRP Annals-Manufacturing Technology, 42(1), 581-583.

[24] Pschl U., 2005. *Atmospheric aerosols: composition, transformation, climate and health effects*, Angewandte Chemie International Edition, 44(46), 7520-7540.

[25] Mercer C. R. & Creath K., 1994. "Liquid crystal point-diffraction interferometer", *Optics Letters*, 19(12), 916-918.

[26] Smartt R. N. & Steel W. H., 1975. "Theory and Application of Point-diffraction Interferometers", *Japan. J. appl. Phys.*, 14, 14-21.

[27] Augustine S. M. & Chetty N., 2014, *Experimental verification of the turbulent effects on laser beam propagation in space*, Atmósfera, 27(4), 385-401.

Chapter 3

EXPERIMENTAL SETUP AND ANALYSIS

3.1 Design

The experimental design used in this work has been adapted from a previous work by Augustine and Chetty [1]. Modifications to the previous setup come in the form of a new turbulence chamber and heater as well as higher precision measuring equipment. Figure (3.1) provides a graphical view describing how the parameters of mach, temperature, pressure and area will be affected between the two types of designs. Our choice of turbulence chamber resembles a subsonic tunnel design since the air density remains almost constant. By constructing the cross section to a smaller size, the air flow will cause an increase in velocity and decrease in pressure which means that with a slightly smaller cross section, we can achieve slightly higher wind speeds while keeping the pressure almost constant.

The alternative design is the supersonic tunnel design since the air density in the tunnel compresses before reaching the testing region. This results in the flow of air decreasing in velocity but increasing in pressure. This is counterintuitive since it does not model the atmosphere which we wish to recreate. In general, the atmospheric pressure varies only slightly over the same altitude and hence we do not wish to cause pressure fluctuations during simulation. Therefore the wind tunnel design used in this work will have a smaller cross section which will increase the velocity of the flow and not the pressure.

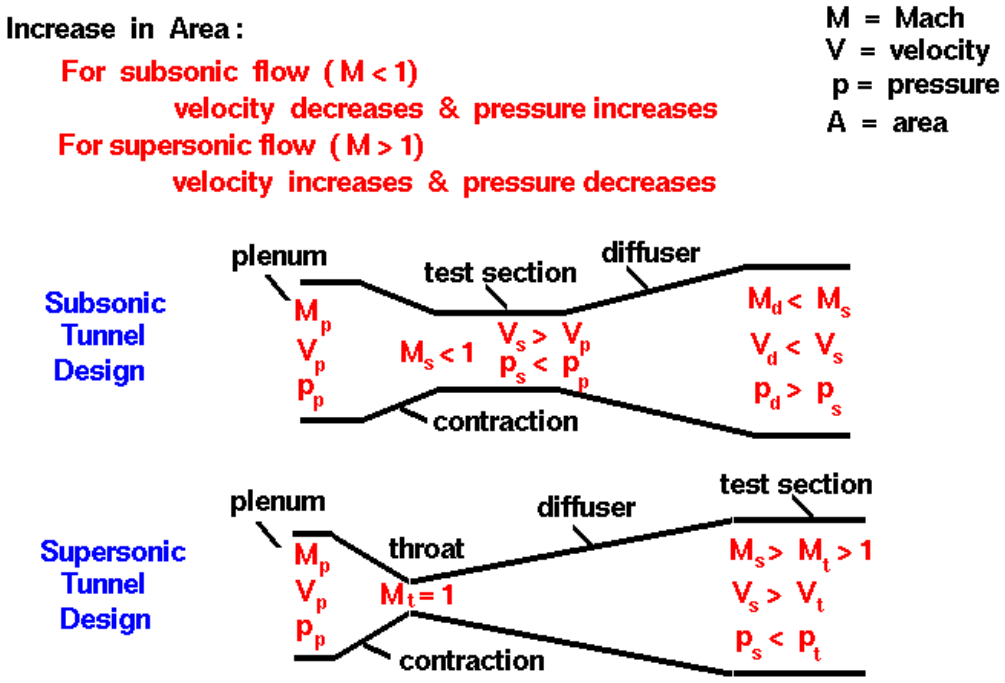

Figure 3.1: Types of wind tunnel designs [2]

Chapter 5 provides details of the new setup and graphical descriptions of the turbulence chamber.

3.2 Analysis

3.2.1 Experimental methods

The experimental procedure involves the running of the experiment, collection of data, calculation of results and analysis thereof. All data have been averaged after all measurements were taken to reduce the experimental error.

The interferograms reported in Chapter 5 have each been through an analysis procedure whereby fast Fourier transforms (FFT's) were applied to break the interferogram into its constituent magnitude and phase regimes. This is necessary to get a better understanding of the actual image since the magnitude regime will provide all the frequencies which compose the image and the phase will provide the phases of the corresponding frequencies. The interferograms are highly sensitive to changes in conditions experienced by the laser beam. Changes in intensity distribution, peak power, shape and blur are detected and can be measured to draw conclusions under specific conditions.

This area is covered in greater detail in Chapter 5, section 1.5. An example has been provided in Figure (3.2), where an unperturbed interferogram has been split into both components. On inspection of the magnitude image, a central bright spot is clearly defined. It symbolises the zero frequency or the largest localisation of frequencies in the image. The central gray localisation implies that there is a large distribution of lower spatial frequencies and decreasing outwards. These

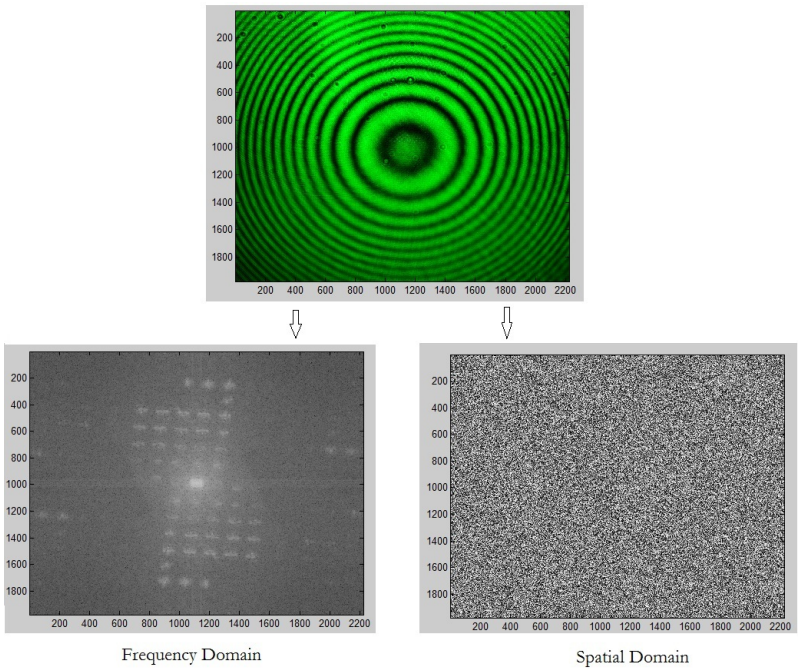

Figure 3.2: Fast Fourier tranform applied to unperturbed interferogram

findings can be substantiated by Figures (3.3) and Figures (3.4) which show how the intensity plot defines a somewhat Gaussian distribution and the contour plot which defines a similar pixel trend. The central dip in the intensity plot can be attributed to one of two reasons, the first being stay artifacts which exist as a result of neutral density (ND) filters removing the highest frequencies in the image or secondly, attenuation of the laser beam as a result of the point discontinuity at the PDI. The phase image does not provide any additional data which would add value to our results. Hence we restrict ourselves to the magnitude regime.

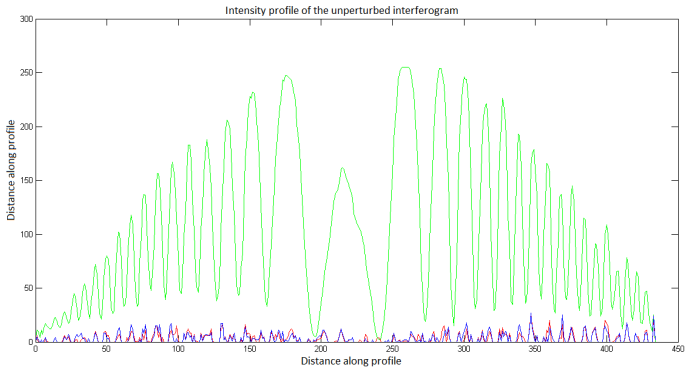

Figure 3.3: Intensity plot of unperturbed interferogram

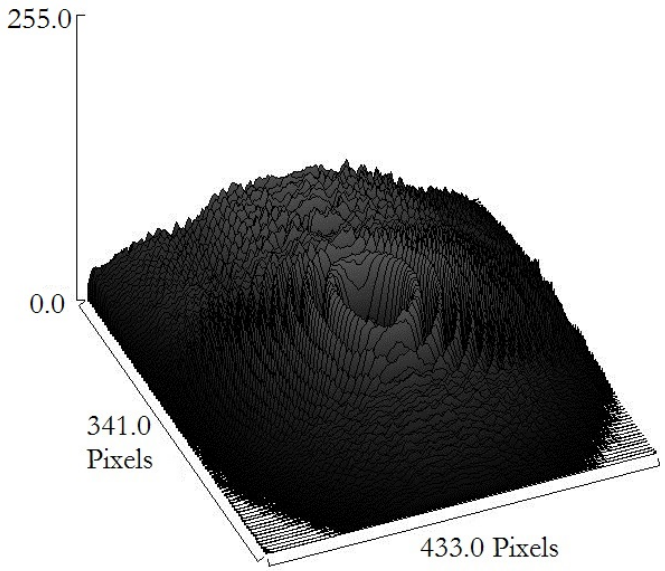

Figure 3.4: Contour plot of unperturbed interferogram

3.3 Results

All published results have been presented in Chapter 5. A sample calculation has been provided below for all the calculated data namely C_n^2, r_0 and R_e from Chapter 5, section 6. Only Reading 1 has been calculated below. The same calculation process will apply to the other readings. To determine C_n^2, equation 1 and equation 2 from section 2, chapter 5 have been combined,

$$C_n^2 = \left(79.0 \times 10^{-8} \left[\frac{\mathrm{p}}{\mathrm{T}^2}\right]\right)^2 \times \left(\left(\sqrt{<(\mathrm{T}_1 - \mathrm{T}_2)^2>}\right)\mathrm{r}^{-1/3}\right)^2 \quad (3.1)$$

$$= \left[\left(79.0 \times 10^{-8} \left[\frac{542.0}{273.0^2}\right]\right)^2\right] \times \left[\left(\sqrt{(23.14 - 24.06)^2}\right) \times \left(\frac{72}{1000}\right)^{-1/3}\right]^2 \quad (3.2)$$

$$= 1.16 \times 10^{-16}\,\mathrm{m}^{-2/3} \quad (3.3)$$

To determine Fried's parameter r_0, equation 4 from section 2, chapter 5 was used,

$$r_0 = 0.185 \left[\frac{\bar{\lambda}^2}{\int_0^z C_n^2(h)dh}\right]^{3/5} \quad (3.4)$$

$$= 0.185 \left[\frac{(0.53 \times 10^{-6})^2}{\int_0^{2.523} 1.16 \times 10^{-16}}\right]^{3/5} \quad (3.5)$$

$$= 8.13\,\mathrm{cm} \quad (3.6)$$

The Reynolds number has been calculated using equation 3 from section 2, chapter 5 was used,

$$\mathrm{Re} = \frac{VL}{\nu} \quad (3.7)$$

$$= \frac{24.8 \times 2.523}{1.983 \times 10^{-5}} \quad (3.8)$$

$$= 5.5 \times 10^5 \text{ dimensionless.} \quad (3.9)$$

References

[1] Augustine S. M. & Chetty N., 2014, *Experimental verification of the turbulent effects on laser beam propagation in space*, Atmósfera, 27(4), 385-401.

[2] https://www.grc.nasa.gov/www/k-12/airplane/Images/tunnozd.gif viewed 20 July 2016.

Chapter 4

CHALLENGES

Despite having achieved the final result in due time, numerous challenges hindered the completion of the work. Some challenges were resolved easily while others took months. Some of the notable challenges have been described below.

The initial challenge was attempting to recreate a stable atmospheric environment in the laboratory. This had on many occasions proven to be a difficult task to achieve. The laboratory used in this work was susceptible to contamination from uncontrollable factors such as dust and particulate which entered through any gaps in the room. This required the use of foam and other materials to seal areas which could cause contamination. In addition, equipment had to be covered and carefully cleaned after every few days to ensure that equipment were performing to their peak capabilities at any time. The cleaning process entailed using special lens wipes to clean the neutral density filters, spatial filter, collimators and camera lenses. The lenses were cleaned once a week irrespective of whether they were dusty or not, this ensured that the results were consistent. The height adjustable rails

were cleaned once every 2 weeks using a dry cloth.

With the room free from external inhomogeneities, the task of setting up and aligning the components also proved to be difficult at times. Since the optical components were highly sensitive to motion, we had to ensure that the setup was on a stable table which did not react to any movements such as vibrations or knocks. If however the setup was bumped or moved, realignment had to occur which took up time.

The design of the wind tunnel proved to be a relatively simple build. The individual components, namely the fan blades, coils and wiring were put together by our in-house electronics department. The components were then enclosed in a heat resistant housing. The tunnel design was precisely measured and cut from PVC plastic. The tunnel was then fixed onto the housing, producing a single component.

During the initial simulations we found that the laser beam dipped in intensity. We found that the problem lied in the original power supply of the laser which was a rechargeable battery powered source. The solution to the was to convert the power supply to run off of an uninterrupted 5V DC source. This solved the issue completely and provided stable laser power.

The last challenge faced was that the heat generated by the turbulence chamber

caused an overall rise in the temperature of the laboratory after a few simulations (15 minutes). This meant that only a few runs could be achieved at a time. To compensate, we allowed equipment and the room to cool until the thermometer dropped to the initial starting temperature. Despite these limitations, the results were unaffected since our laboratory was on site and could be used freely.

4.1 Discussion

Our atmosphere consists of inhomogeneities which come in all shapes and sizes. A laser beam propagating through the atmosphere will experience random fluctuations in beam shape, size, position and intensity. The extent to which the beam is affected depends on the path length traversed, the actual strength of the turbulence and the wavelength of the laser beam itself. Chapter 5 provides a complete journal article submitted to and accepted by Atmósfera. The experimental setup has proved to be successful in its ability to reproduce the desired atmosphere. The new turbulence generator in the form of a heated wind tunnel was also successful in developing various levels of perturbations and inevitably allowed us to conduct a series of measurements which modeled minimal to highly turbulent atmospheric conditions. The measured data for C_n^2 has coincided well with published works with some variance being attributed to geographical location. Notable works by [1–4] have presented contrary results to ours however propagation distances and turbulence sources vary drastically from those used in this work. For instance [3] has propagated a He-Ne laser through earths atmosphere over a path length of 1.25 km. Since the simulation takes place in the open atmosphere, the atmosphere

is highly unstable which means that the results will vary at different times of the day. For this reason, comparing results here would be inconclusive and hence we have compared our results to a variety of sources to draw an overall conclusion of whether our data falls within expectation.

Other measured characteristics were Fried's parameter which has shown to fare well with expected results and has shown to decrease with an increasingly turbulent atmosphere [4]. Results for the flow in the form of Reynolds number has shown to increase in relation to an increase in wind speed. In addition, we found that the Reynolds number did not have a large dependency on temperature which we look to explore further in future works. Other improvements/upgrades which we wish to employ involve a new turbulence source in the form of a heated water bath; assess the impacts of turbulence on different lasers such as a CO_2 or Argon laser and, increase the speed at which we can obtain a straight line accuracy through the components. These upgrades will provide us with new data on laser beams as well as optimize our design for quicker and efficient data collection.

In conclusion, the importance of this work is predicated upon having a thorough knowledge of lasers and their behaviour through a turbulent atmosphere. Understanding the behaviour of a laser under these conditions will allow us to effectively harness the full capabilities of the laser as well as the apparatus we use to classify it. Using the results of this work, we inevitably want to achieve two main outcomes, the first showing the simplicity and efficiency of our experimental

setup and the second, being able to fully classify the laser beam under turbulent conditions so that the results can assist industry and research technology in further improving or developing laser applications.

References

[1] Gamo H. & Majumdar A.K., (1978). "Atmospheric turbulence chamber for transmission experiment: characterisation by thermal method," *Appl. Opt.*, 17, 3755-3762.

[2] Gochelashvili K., (1971). "Saturation of the Fluctuations of Focused Radiation in a Turbulent Medium," *Radiophys. Quant. Electron*, 14, 470-473.

[3] Parry, G., 1981. Measurement of atmospheric turbulence induced intensity fluctuations in a laser beam. Journal of Modern Optics, 28(5), pp.715-728.

[4] Magee E. P., 1993. *Characterisation of Laboratory Generated Turbulence*, MSc Thesis, Air Force Institute of Technology, United States.

Chapter 5

WIND TUNNEL SIMULATIONS TO DETECT AND QUANTIFY THE TURBULENT EFFECTS OF A PROPAGATING HE-NE LASER BEAM IN AIR*

*Augustine S. M. and N. Chetty, 2016. Wind tunnel simulations to detect and quantify the turbulent effects of a propagating He-Ne laser beam in air. *Atmósfera*, 27(4), in press.

Wind tunnel simulations to detect and quantify the turbulent effects of a propagating He-Ne laser beam in air

S Augustine and N Chetty[1]

University of KwaZulu-Natal, School of Chemistry and Physics,

Pietermaritzburg, Scottsville 3201, South Africa

[1]ChettyN3@ukzn.ac.za

ATMOSFERA

Mexico City, November 11, 2016

Mr. Shivan Michael Augustine
University of KwaZulu-Natal
South Africa

Dear Mr. Augustine:

I have the pleasure to inform you that your manuscript *Wind tunnel simulations to detect and quantify the turbulent effects of a propagating He-Ne laser beam in air*, by Shivan Michael Augustine and Naven Chetty, has been accepted for publication in ATMÓSFERA.

On behalf of the Editorial Committee, I appreciate you have considered ATMÓSFERA to present your scientific work.

Sincerely yours

Dr. Carlos Gay
Editor

Wind tunnel simulations to detect and quantify the turbulent effects of a propagating He-Ne laser beam in air

S. M. Augustine and N. Chetty[1]

School of Chemistry and Physics, University of KwaZulu-Natal, Pietermaritzburg, South Africa, 3201

[1]*ChettyN3@ukzn.ac.za*

Abstract: In this paper, we ascertain the effectiveness of our experimental setup in detecting and quantifying the turbulent effects experienced by a He-Ne laser beam as it passes through a wind tunnel. The beam propagated through a series of optical components as well as the in-house deigned and manufactured wind tunnel under controlled laboratory conditions. The wind tunnel was built to fit within an existing setup which has previously proven to be successful in detecting the turbulent effects from other turbulence models. For various wind speeds and temperature settings, the setup has been successful as it was able to detect and measure the atmospheric conditions within the turbulent environment and fully quantify the characteristics of the laser beam. With the use of highly accurate measuring devices, we were able to successfully measure the refractive index structure function (C_n^2) and the coherence diameter (Fried's parameter). Values for C_n^2 ranged between $1.61\times10^{-16}\,\mathrm{m}^{-2/3}$ and $6.77\times10^{-15}\,\mathrm{m}^{-2/3}$ which can be classified under the moderate to strong turbulence regime. These results tie in well with various published works for similar atmospheric scenarios hence this setup was successfully able to fully detect and quantify the thermal turbulence and wind velocity effects on the laser beam using a point diffraction interferometer.

Nomenclature

C_n^2 - Refractive index structure function ($m^{-2/3}$)

C_T^2 - Temperature structure function ($K^2 m^{-2/3}$))

FFT - Fast Fourier transform

He-Ne - Helium Neon

k - Wavenumber (nm)

L - Propagation path length (m)

p - Pressure (kPa)

PDI - Point diffraction interferometer

r - Length between two reference points (m)

R_e - Reynolds number (dimensionless)

r_0 - Fried's parameter (cm)

T_1 and T_2 - Temperatures at two reference points (K)

u - Mean velocity ($m.s^{-1}$)

ν - Kinematic viscosity ($m^2.s^{-1}$)

°C - Degrees Celcius

1. Introduction

In the atmosphere, the implications of meteorological conditions imposes significant effects on optical image testing (Andrews and Ronald, 1998). Due to the limitations involved in controlling the in-situ atmospheric conditions, lab experiments are considered using standard environmental conditions. In this study, we investigate the influences of aerodynamic disturbances on image quality using a point diffraction interferometer (PDI).

Research has shown that refractive index fluctuations of the atmosphere are significant near the surface of the Earth and negligible at higher altitudes (Andrews and Phillips, 1988). These refractive index fluctuations cause random phase perturbations of the laser beam which can lead to beam distortion (Chatterjee and Fathi, 2014). This paper aims to determine the effectiveness of using a PDI to measure variations in thermal turbulence generated using a heated wind tunnel. The model is an extension to work previously done by (Augustine and Chetty, 2014) as it has proven to be robust, cost efficient and stable in detecting and fully quantifying the effects of thermal turbulence on laser beam propagation in air. In-situ simulations have described the difficulty involved in setting up field experiments to measure atmospheric conditions (Magee 1993, Kemp *et al* 2001, Hona J *et al* 2008, Smartt R. N. & Steel W. H. 1975). Works by (Carnevale M *et al* 2013, Carnevale M *et al* 2014, Montomoli F *et al* 2015) have used numerical approaches to model turbulence and have explained the importance of using experimental means to justify their findings. The instability of the atmosphere requires extremely expensive and sophisticated equipment to measure and characterise the atmosphere. For this reason, modeling the atmosphere in a laboratory has been the preferred method since specific conditions can be controlled while others are measured. In this way, we have been able to produce highly comparable results as shown in literature using relatively cheaper and robust equipment (Gamo 1978, Gochelashvili and Shishov 1974, Magee 1993).

A wind turbine has been designed to simulate the effects of atmospheric

turbulence. The turbulence generator incorporates a wind tunnel which consists of a heating element and a single fan with two speed settings. The effects of the turbulence experienced by the laser beam has been measured using a PDI which produced interferograms for analysis. The statistical properties of the interferogram is thereafter processed and analysed. The setup incorporates a high speed wind turbine with a heated element capable of generating winds between 20.8km/h and 28.5km/h. To detect all the different factors influencing the beam, we made use of an Bruton ADC Pro anemometer to measure the wind speed, an in-house developed pressure sensor to accurately detect the pressure within the turbulent region and a thermocouple to measure the temperatures at reference points. The high sensitivity of these devices allowed any slight variations in pressure, temperature and wind speed to be accurately measured between the turbulent and non turbulent regions. The primary light source used in this work was a green continuous wave He-Ne 532 nm laser. To determine the effect of thermal turbulence on laser beam propagation, a complete analysis of the produced interferograms at various temperatures has been discussed using advanced image analysis software. In addition, various characteristics of the atmosphere have been determined namely, the temperature, temperature structure function, pressure, air velocity, refractive index structure function and Fried's parameter.

2. Theory

Whilst determining the effectiveness of using a point diffraction interferometer to measure wind turbulence, many other atmospheric characteristics can be simultaneously measured and calculated. The refractive index structure function

(C_n^2) is one of the main characteristics which describe the atmosphere (Magee, 1993). The random fluctuations in the refractive index of the atmosphere alter the propagation pathway of light beams which, in turn, effects their initial phase fronts (Andrews and Phillips, 1988). Once light propagates through a turbulent atmosphere, the phase fronts become distorted and experience random changes in beam direction (beam wander) as well as random intensity fluctuations (scintillation) (Berman et al, 2013).

Sophisticated measuring equipment has been used to measure the air temperature and pressure within the turbulent region. The propagation path length is represented by L and is equal to 2.52 m. The wavenumber k is the wavelength of a helium-neon laser at 532 nm. r describes the region between two reference points within the propagation path length. T_1 and T_2 represent the temperatures at the two reference points. Measuring these observations in the laboratory allows one to determine C_n^2 through (Andrews and Phillips, 1988),

$$C_n^2 = \left(79.0 \times 10^{-6} \left[\frac{\mathrm{p}}{\mathrm{T}^2}\right]\right)^2 \mathrm{C}_T^2, \tag{1}$$

with

$$C_T^2 = \left(\sqrt{< (\mathrm{T}_1 - \mathrm{T}_2)^2 >}\right)^2 \mathrm{r}^{-2/3}, \tag{2}$$

where C_T^2 represents the temperature structure function.

As the laser beam propagates through the inhomogeneous medium, the turbulence created within the wind tunnel presents itself as small packets of air, also known as turbulent eddies. Each turbulent eddie has a unique refractive index

which affects the laser beam differently. Holistically we can obtain the general strength of the turbulent region using equation 1. Typical values of C_n^2 range from $10^{-17}\mathrm{m}^{-2/3}$ or less for weak turbulences and $10^{-13}\mathrm{m}^{-2/3}$ or more for strong turbulence (Andrews and Phillips, 1988 and Weichel, 1990). Other characterising features of the atmosphere can also be classified by the Reynolds number and seeing conditions (Fried's parameter). The Reynolds number is given by,

$$R_e = \frac{u\,l}{\nu}, \tag{3}$$

where, u is the mean velocity, ν is the kinematic viscosity of the fluid and l, the path length. We can relate the index function to Fried's parameter through (Magee, 1993),

$$r_0 = 0.185 \left[\frac{\bar{\lambda}^2}{\int_0^z C_n^2(h)dh} \right]^{3/5}. \tag{4}$$

Determining the seeing conditions at low altitude may result in very low values (less than 5cm) as the quantity alone describes the quality of the optical signal through the atmosphere. At high altitudes such as an observatory which is clear from high levels of atmospheric contrasts, should yield values of r_0 between 5cm and 20cm.

3. Experimental Setup

A diagrammatic description of the components is presented in Figure (1)

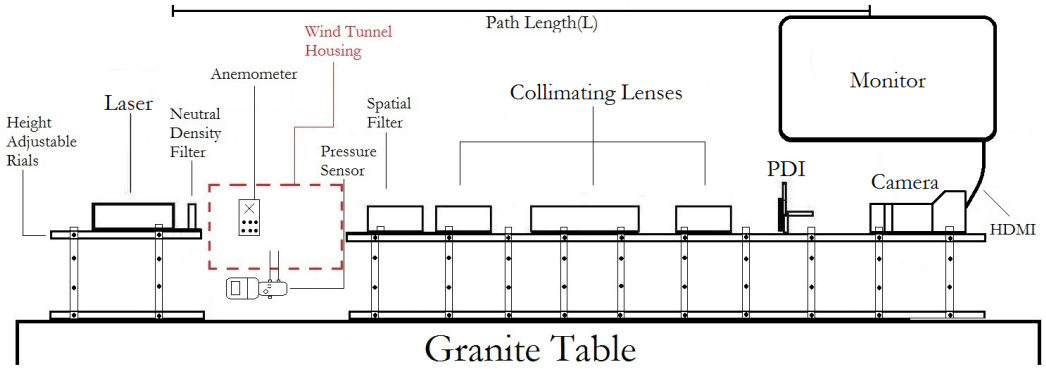

Fig. 1: 2D view of the experimental setup

A more detailed design of the wind tunnel is presented in Figure (2)

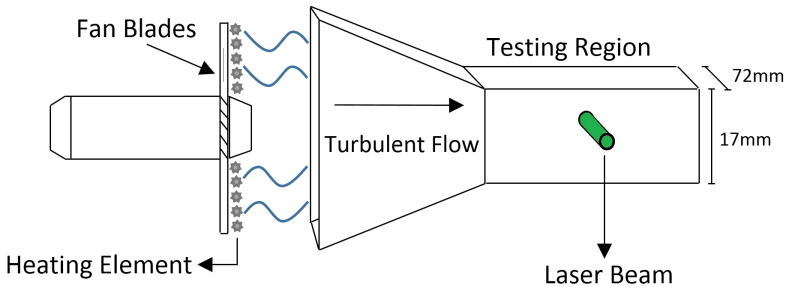

Fig. 2: Depiction of the wind tunnel

The experimental setup used in this work was adapted from a previous work by (Ndlovu and Chetty, 2013). We have chosen to use a laboratory setup as it removes the inconsistency of the atmosphere such as varying wind velocities, temperatures and flow directions. Once the setup is able to detect and quantify the effects of simulated atmospheric turbulence, the setup can be moved outside.

A turbulence generator and chamber have been designed for the laboratory setup but the characteristics of the turbulence generator are designed to mimic real world atmospheric turbulence. By introducing a wind element into the setup, a new technique for characterising the laser beam will be explored. As with previous works by (Augustine and Chetty 2014, Ndlovu and Chetty 2013), we set out to minimize the cost and time devoted into our testing procedures. To recreate atmospheric wind, a fan connected to a high powered motor was used. The fan blades spin at high velocity producing a consistent stream of air which propagates perpendicularly to the motion of the laser beam. The air was immediately heated by a coil which can be operated at two power settings, 1000 W and 2000 W. The characteristics of air speed, air temperature and pressure were measured at the exit of the tunnel at a distance of 36mm along the length (Refer to Figure 2). The resultant perturbed beam was then photographed and the statistical properties of the perturbation thereafter measured.

4. Experimental Procedure

The optical components were first checked to ensure that they are free of any dust particles. The laser is thereafter given sufficient time to warm up and stabilize. The laser alignment is also checked so that it propagates directly through the optical components. The wind turbine was given sufficient time to run before measurements began. The heating element had four possible settings. Table 1 describes each setting and provides the temperature and corresponding characteristics of the wind tunnel.

Setting Number	Wind Speed(km/h)	Temperature(°C)	Pressure(Pa)
1	24.8	24.06	542
2	28.5	27.06	765
3	20.8	48.89	522
4	26.5	55.21	734

Table 1: Table of wind speed versus temperature

Settings 1 and 2 represent two variations in wind speed with no additive heat, i.e. high velocity room temperature wind. It was necessary to determine if there was any influence on the laser beam with the element of heat removed. The results are presented in section 5.

5. Results, analysis and discussion

5.1. Reading 1

For comparison, the unperturbed interferogram is presented in Figure (3).

Fig. 3-Unperturbed interferogram

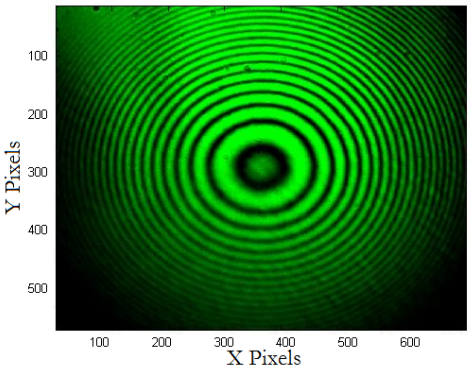

Fig. 4-Unperturbed intensity distribution

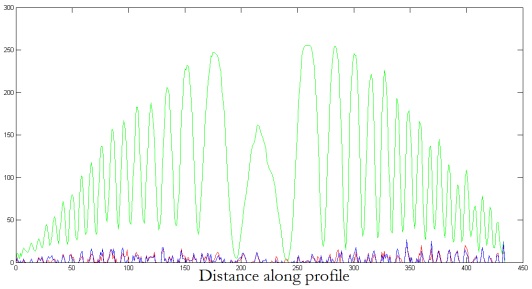

Fig. 5-Magnitude of the FFT

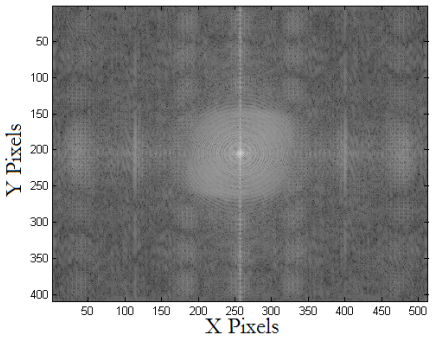

Fig. 6-Point spread function

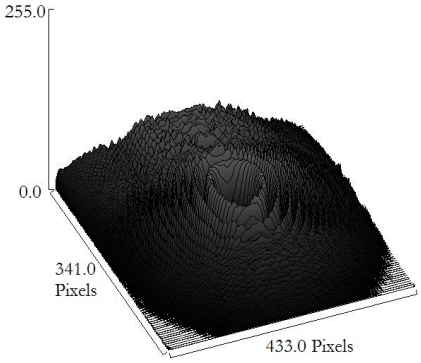

Figures 3 to 6 present the results for the unperturbed interferogram

Reading 1 will be the basis of comparison against the other readings as it represents a laser beam propagating through a homogeneous medium with no applied turbulence (thermally or directionally). Determining the differences in the interferograms, intensity profiles, Fast Fourier Transforms (FFT) and image subtractions will provide us with insight into how the laser beam reacts under low and high turbulent strain. The turbulence generated in the laboratory could typi-

cally represent aerodynamical configurations experienced in the atmosphere by airbourne platforms (Magee, 1993). Figure (3) presents a clearly defined interferogram which exhibits a uniform distribution of energy over the area of the laser beam. Figure (4) expresses the intensity profile which resembles a Gaussian profile which is expected since the beam is unperturbed. The dip in the centre can be attributed to stray artifacts arising from either the neutral density or spatial filter. Figure (5) is the FFT which was used as it resolves the image into its magnitude and phase domains. The magnitude is useful for image processing since all the frequencies which compose the image are specified. We will restrict ourselves to the magnitude domain as the frequency domain does not provide us with sufficient information. Making reference to Figure (5), the image is formed on a 2D plane in polar representation and shows that there is a high concentration of frequencies at the centre of the image. The image contains various frequency components which decrease slowly for larger frequencies. The central bright spot is known as the zero frequency zone or direct current zone and represents the average colour value of the entire image (Banish, 1990). Additionally, the image does not contain imaginary components and, thus, the magnitude at the centre has a zero phase resulting in a gray spot. The large concentration around the centre point indicates a lower spatial frequency (Banish, 1990). Numerous adjustments can be made to the transformed image to either improve the focus or decrease blurriness and this can be achieved by applying a low pass filter to preserve the low frequency regions, or a high pass filter, to preserve the sharpness and defined edges. Intermittent filters can be applied and are known as band pass filters. For comparisons in subsequent readings we will compare their FFTs to Figure (5) by image subtraction. If the subtraction yields

a completely black image then it is implied that the two images coincide completely and, hence, there is no change in beam position, distortion, blurriness or phase.

5.2. Reading 2

Setting 1 describes the scenario of a moderately windy day at 20.5°C.

Fig. 7-Setting 1-Perturbed interferogram

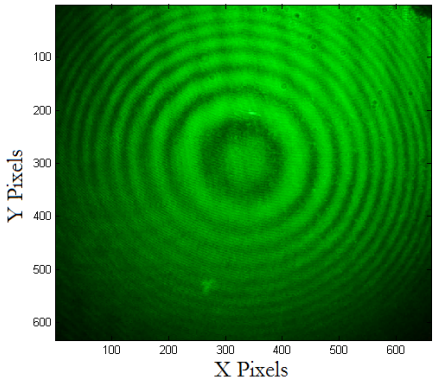

Fig. 8-Setting 1-Intensity distribution

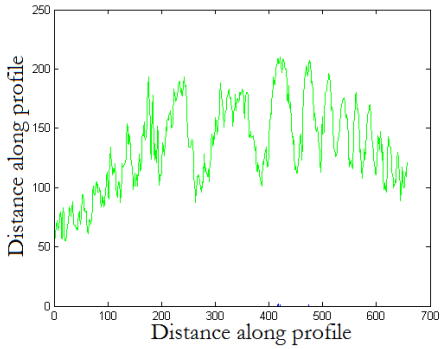

Fig. 9-Setting 1-Magnitude of the FFT

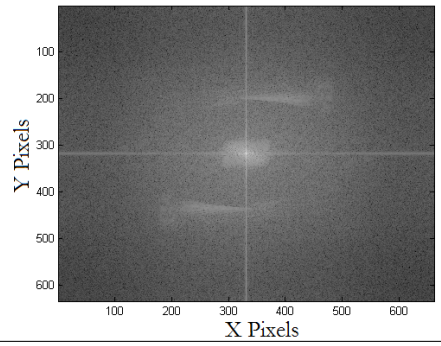

Fig. 10-Setting 1-Image subtraction

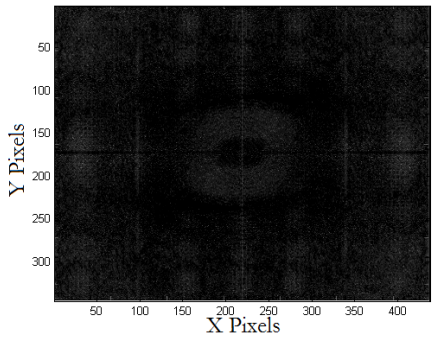

Figures 7 to 10 present the results for the perturbation at turbulence setting 1

The results displayed are those of the perturbed laser beam being exposed to 24.8km/h wind velocity at a room temperature of 24.06°C. In Figure (7) we can see that the dark fringes are less defined and that the interferogram is blurred

when compared to Figure (3). Figure (8) shows an energy redistribution over the area of the interferogram and also shows a maximum peak intensity of 220 units over the initial unperturbed value of 255 units. Although the intensity is only 35 units lower, there is a total redistribution of energy over the peaks. The FFT magnitude in Figure (9) shows a small collection of the lower spatial range in the centre, which infers a somewhat similar spatial distribution as the unperturbed beam. This means that despite the distortion and blurriness of the interferogram, the spatial domain has been altered (Banish, 1990). Compared to Figure (5), the collection of lower frequencies is significantly less but not entirely substantial. The image subtraction data in Figure (10), shows us the lower spatial region which has been either shifted to higher frequencies or lost during propagation. Overall, the beams characteristics are still strong and possesses qualities of its initial form.

5.3. *Reading 3*

Fig. 11-Setting 2-Perturbed interferogram

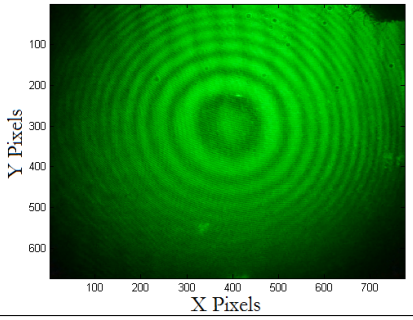

Fig. 12 -Setting 2-Intensity distribution

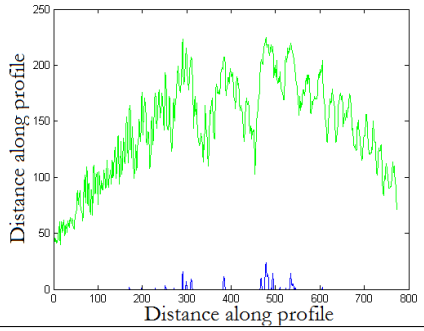

Fig. 13-Setting 2-Magnitude of the FFT

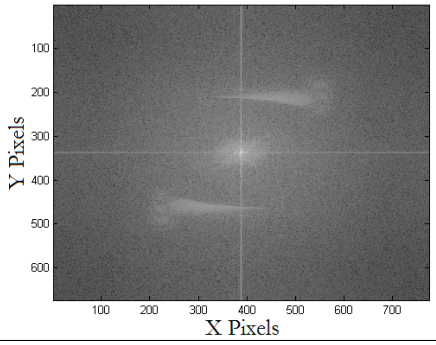

Fig. 14-Setting 2-Image subtraction

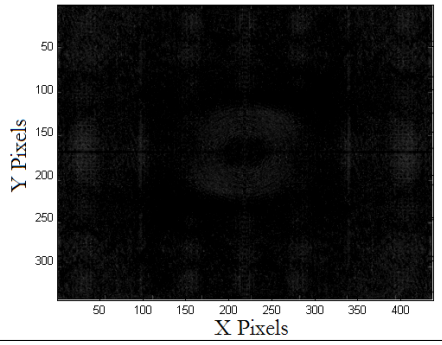

Figures 11 to 14 present the results for the perturbation at turbulence setting 2

Reading 3 was conducted at the highest speed setting achievable by the wind turbine at 28.50km/h and at a room temperature of 27.06°C. The higher room temperature is due to the much higher ambient temperature within the laboratory. Despite the increase in turbine speed, the changes visually are the most significant. Propagation path length and altitude remain the same as in other testings. The fringes are slightly lighter signifying that the beam is experiencing directional fluctuations and is shifting over the PDI membrane. The intensity profile in Figure (12) shows approximately the same drop in peak power as in Figure (8). Additionally, the FFT magnitude Figure (13) and image subtrac-

tion Figure (14) present similar data to reading 1. This implies that the beam suffered minor changes with an increase in wind speed of 3.7km/h. The high localisation of the lower spatial region implies minimal directional deviation from the initial unperturbed interferogram. The image subtraction data shows that the energy as well as directional fluctuations are evident as seen by the gray pixels existing from the middle to centre of the image. Future work will entail building a larger wind tunnel which can simulate wind speeds of up to 100km/h. Small scale tests are necessary to determine if the PDI can measure small scale simulations.

5.4. *Reading 4*

Fig. 15-Setting 3-Perturbed interferogram	Fig. 16-Setting 3-Intensity distribution
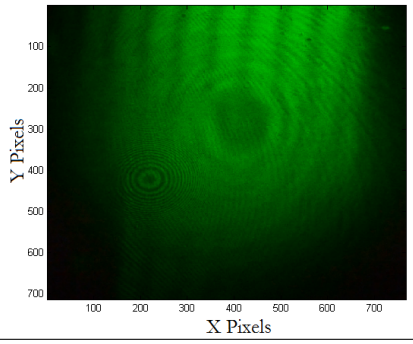	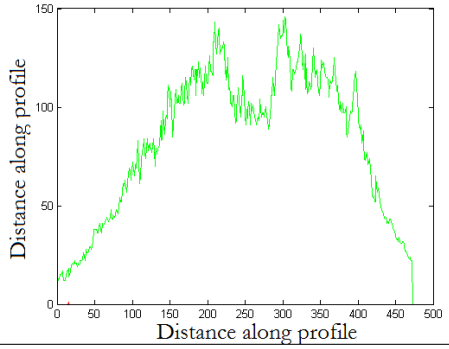
Fig. 17-Setting 3-Magnitude of the FFT	Fig. 18-Setting 3-Image subtraction
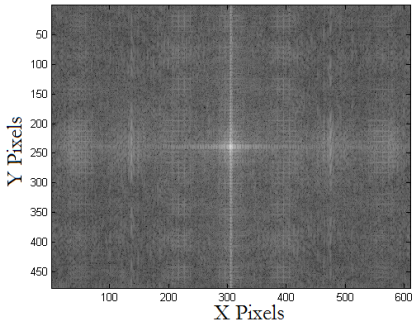	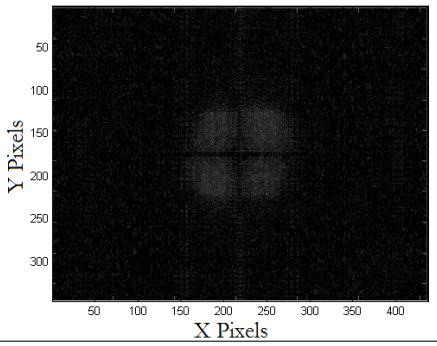

Figures 15 to 18 present the results for the perturbation at turbulence setting 3

Reading 4 made use of a single 1000W coil which heated the air significantly to 48.89°C and at a wind velocity of 20.8km/h. After approximately 10 minutes readings were taken and averaged. The interferogram in Figure (15) describes a severely distorted, blurred image. The fringes are completely deformed, faint and out of focus when compared to the unperturbed interferogram. The directional shift of the laser beam has caused the laser to propagate through more than one PDI pinhole hence causing the constructive and destructive fringes. The intensity profile in Figure (16) shows that the peak intensity reaches 145 pixel units from a maximum value of 254 pixel units. A drop of 43% in inten-

sity. Despite the somewhat Gaussian distribution, it is interesting to note that the intensity is redistributed over the beam. The image subtraction Figure (17) shows an almost absent lower spatial region. The frequencies are random and encompass the entire area of the beam. This signifies a complete redistribution directionally and spatially. Work by (Banish, 1990) has described this behaviour to result in image blur and deformation which is evident from the interferogram. Figure (18) presents the difference in the lower spatial localisation from the initial unperturbed data. This simulation has caused the beam to lose many of the basic characteristics of a He-Ne laser such as having a high coherence and directional forte. However, the energy distribution is still discribing a Gaussian profile but with significantly less energy.

5.5. Reading 5

Fig. 19-Setting 4-Perturbed interferogram

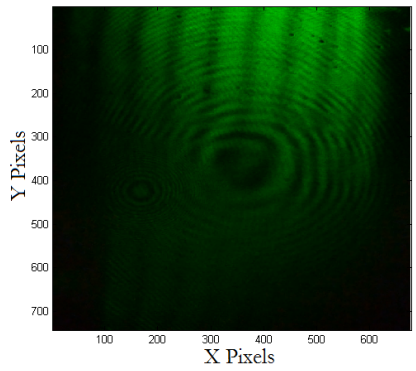

Fig. 20-Setting 4-Intensity distribution

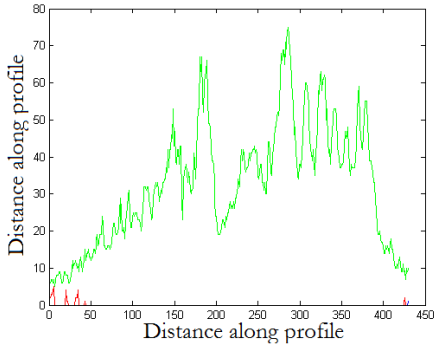

Fig. 21-Setting 4-Magnitude of the FFT

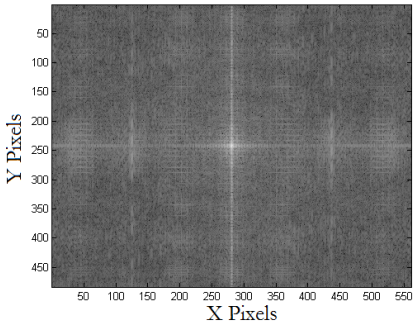

Fig. 22-Setting 4-Image subtraction

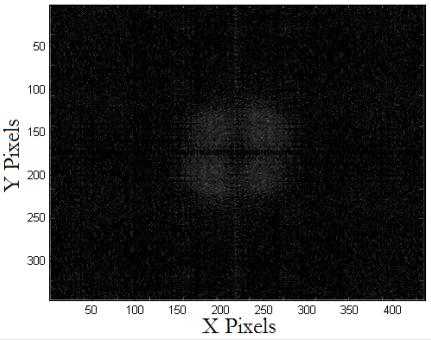

Figures 19 to 22 present the results for the perturbation at turbulence setting 4

Reading 5 utilises the highest speed and temperature capabilities of the wind turbine. Within the turbulent region, the air is heated to 55.21°C and is moving at a velocity of 26.5 km/h. Even though the wind speed has increased only slightly, the 6.3°C heat increase has rendered the laser beam to be almost completely unidentifiable. Figure (19) describes a highly affected beam which has no focus, shape or form. This is due to its loss of coherence, direction and intensity. It is interesting to note how quickly the laser beam completely loses its basic characteristics with an increase in temperature variation. The intensity

profile Figure (20) resembles an erratic trend which suggests that the beam has experienced various energy redistributions over the entire profile. The peak intensity has dropped to 76 pixel units from the original value of 254 pixel units. This defines an extreme loss in energy of approximately 70%. Figure (21) is the FFT and shows a complete loss of the beams lower spatial frequency just as in reading 4. The phases of the laser beam are inconsistant and do not follow a consistant distribution as would be expected. Figure (5) reinforces the expectations of the He-Ne Gaussian profile to have a defined lower spatial domain (Banish 1990, Fried 1965). The image subtraction data in Figure (22) reveals a grey central region which shows us the difference in the lower spatial frequency redistribution when compared to Figure (5). The exposure of the beam to such heat with wind velocity has caused it to lose all its basic characteristics. In this case the intensity has dropped so low that only 30% of its initial energy has reached the detector. Any further simulations above this temperature may lead to more severe implications and possibly an eventual loss of all the energy.

6. Determination of C_n^2

To measure the refractive index of the atmosphere within the turbulent region, a few parameters are required, namely, the temperature (T_1 and T_2), pressure (p) and separation distance (r=72 mm). In this work, 4 averaged readings were taken. The first 2 being two variations of high wind velocity without additive heat. The second being two variations of wind velocity and heat. Tables 1 and 7 present the parameters,

Reading	T_1 (°C)	T_2 (°C)
1	23.14	24.06
2	23.14	27.06
3	48.89	45.60
4	55.21	50.04

Table 2: Atmospheric parameters

The data in Tables 1 and 7 are used to determine the refractive index structure function, temperature structure function and seeing parameter with the use of equations 1, 2 and 3 respectively,

Reading	C_T^2 ($K^2m^{-2/3}$)	C_n^2 ($m^{-2/3}$)	$r_0(cm)$	$R_e(\times 10^5)$
1	4.89	1.61×10^{-16}	8.1	5.5
2	88.79	4.22×10^{-15}	1.1	6.3
3	62.54	1.39×10^{-15}	2.2	4.6
4	154.44	6.77×10^{-15}	0.8	5.9

Table 3: Temperature and refractive index structure function data

The results in Table 8 compare well with numerous published data for similar atmospheric scenarios (Ndlovu 2013, Tunick *et al* 2005, Weichel 1990, Kemp *et al* 2001). Our results for C_n^2 can be classified under the moderate to strong turbulence regime (Andrews and Phillips, 1988). Our measuring apparatus have allowed us to precisely determine these structure functions accurately. Values for C_n^2 vary from one source to the other and depend largely on the logistics of the atmosphere, the position above ground, the separation distance between measuring points and the consistency of the temperature over the path length. For short path length such as the one used in this experiment, the turbulence can be accurately determined due to the stability of the atmosphere within the laboratory. The seeing parameter ranges between 8.1 cm and 0.8 cm (Kemp *et al* 2001). Decreasing values of r_0 result in increasing phase distortions of the laser

beam as well as an increasing degradation of the atmosphere. This claim has been extensively reviewed in the analysis of readings 2 to 5. Another parameter which is often used to classify the flow of the atmosphere is the Reynolds number. From the data in Table 8, the Reynolds number describes a highly turbulent flow and implies that for a consistent medium, an increase in measured air speed over a measured distance will result in a proportional increase in the Reynolds number.

6.1. Error analysis

The experimental error arises from both systematic and random contributions. Systematic errors occur from the mis-calibration of measuring apparatus. The PDI controller has been quoted at 95% accuracy, hence a maximum error of 5% can be expected. The pressure sensor quotes a maximum possible error of 0.1 Pa or a 1% error. The thermocouple states a precision of 0.1 °C which is approximately a 1% error. The anemometer quotes a 1% total error. Although these errors are expected from the measuring instruments we have averaged our data over thousands of simulations therefore the mean would be an estimate of the true result. Random errors occur through dust particulate in the air, vibrations in the floor or any random air currents exiting during simulations. Our laboratory environment has been sealed off to allow minimal dust, vibration or air currents into the testing region. We can therefore assume a precision accuracy of 95% in our results. The error bar chart of the new C_n^2 range is provideed in Figure (23),

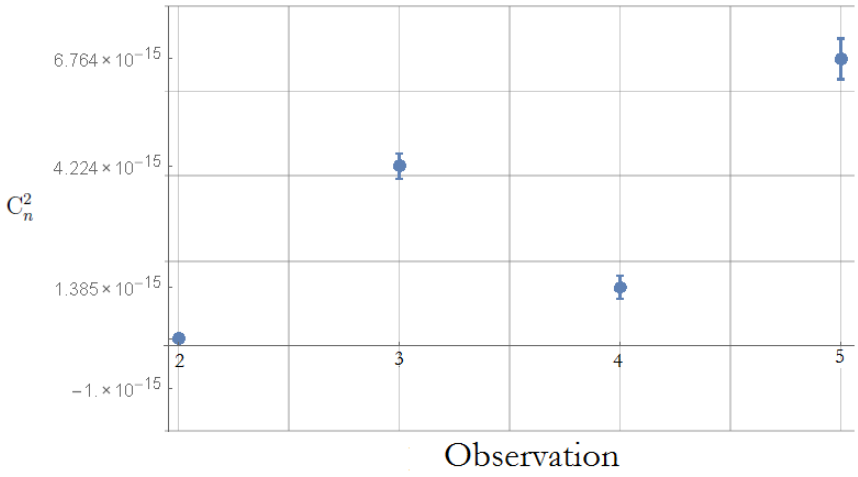

Fig. 23: Refractive index variations for readings 2-5

6.2. Conclusion

Our results prove that the PDI was able to detect and produce quantifiable interferograms. Thousands of readings were taken and averaged into four separate divisions. Two being variations of wind speed at room temperature and the remaining two being two heat settings at two possible wind speeds. All perturbed readings were compared against the unperturbed results to measure the differences and effects. In summary, readings 2 and 3 showed signs of image blur, minor beam wander, minor beam spreadings but both held a strong intensity profile. This implies that wind velocity alone does not destroy all the beams characteristics. Readings 4 and 5 however were severely affected by the accompanying heat included in the wind stream. Both showed an extreme loss of coherence, direction and intensity. Reading 5 exhibited no basic elements of the initial unperturbed analysis and was almost uncharacterisable. Smaller values relate to an increasingly degraded atmospheric. With this in mind, we can conclude that the heat perturbations were significantly more severe than

perturbations with wind velocity alone. The additive effect however has shown a beam to be severely degraded in terms of power loss as well as directional fluctuations. In previous works by (Augustine and Chetty, 2014), data has been provided for a heated panel as a turbulent source. The results vary to this work since the contributions from directional fluctuations were minimal. As such, we can conclude that heat contributions alone do not affect the laser beam as significantly as directional perturbations. To further classify the atmosphere within the turbulent region, we determined the refractive index structure function which ranged from 1.61×10^{-16} to 6.77×10^{-15} which falls under the moderate to strong turbulence regime. The seeing parameter was also calculated and found to lie between 8.1cm to 0.8cm. Future work entails developing a liquid bath through which the laser beam will propagate. We wish to determine how the laser beam reacts through different liquids as well as through varying liquid temperatures. Other detection and analysis methods will also be explored to best suit the experimental design and expectations.

References and Links

Andrews L. and Ronald P., *Laser Beam Propagation Through Random Media*, (Academic, Washington, 1998). http://dx.doi.org/10.1117/3.626196

Andrews L.C., Phillips R.L., Sasiela R.J. and Parenti R., "Beam wander effects on the scintillation index of a focused beam", Proc.SPIE **5793**, (2005). http://dx.doi.org/10.1117/12.604855

Augustine S. and Chetty N., *Experimental Verification of the Turbulent Effects on Laser Beam Propagation in Space*, Atmra, (27) 4, 385-401, (2014). http://dx.doi.org/10.1016/S0187-6236(14)70037-2

Banish M. R., R.L. Clark and A.D. Kathman, "Wavelength dependence of blur circle size through turbulent flow", Window and Dome Technologies and Materials II, Proc. of SPIE **1326**, 196-206 (1990). http://dx.doi.org/10.1117/12.22500

Berman G.P., Chumak A.A. and Gorshkov V. N., *Beam Wandering in the Atmosphere:The Effect of Partial Coherence*, (Academic, Ukraine, 2013).

Carnevale, M., *et al.*, *Uncertainty quantification: A stochastic method for heat transfer prediction using LES*, Journal of Turbomachinery **135**, 5 (2013). http://dx.doi.org/10.1115/1.4007836

Carnevale, Mauro, *et al.*, *Film Cooling and Shock Interaction: An Uncertainty Quantification Analysis With Transonic Flows*, ASME Turbo Expo 2014: Turbine Technical Conference and Exposition. American Society of Mechanical Engineers (2014). http://dx.doi.org/10.1115/GT2014-25024

Chatterjee R.M. and Fathi H.A.M., "Investigation of profiled beam propagation through a turbulent layer and temporal statistics of diffracted output for a modified von Karman phase screen," Proc. SPIE **897102**, 897102-897102-16 (2014).

Hona J, Elisabeth N.N and Elkana P. “Experimental technique using an interference pattern for measuring directional fluctuations of a laser beam created by a strong thermal turbulence,” Progress In Electromagnetics Research **84**, 289-306 (2008). http://dx.doi.org/10.2528/PIER08072803

Kemp E.M., Felton B.D., and Alliss R.J., P9. 30 “Estimating the refractive index structure function and related optical seeing parameterswith the WRF-ARW (2001).”

Fried, D.L., “Statistics of a geometric representation of wavefront distortion”, *JOSA*, 55(11), 1427-1431 (1965). http://dx.doi.org/10.1364/JOSA.55.001427

Gamo H. and Majumdar A.K., “Atmospheric turbulence chamber for transmission experiment: characterisation by thermal method,” Appl. Opt., **17**, 3755-3762 (1978). http://dx.doi.org/10.1364/AO.17.003755

Gochelashvili K. and Shishov V., “Saturated Intensity Fluctuations of Laser Radiation in a Turbulent Medium,” Zh. Eksp. Teor. Fiz **66**, 1237-1247 (1974).

Magee E. P., 1993. Characterisation of Laboratory Generated Turbulence, MSc Thesis, Air Force Institute of Technology, United States.

Montomoli F, *et al.*, *Uncertainty Quantification in Computational Fluid Dynamics and Aircraft Engines*, Springer Briefs in Applied Sciences and Technology, (2015). http://dx.doi.org/10.1007/978-3-319-14681-2

Ndlovu S., *Experimental Measurement of the Fluctuations of Laser Beam Due to Thermal Turbulence*, MSc thesis, University of Natal, South Africa (2013).

Smartt R. N. and Steel W. H., “Theory and Application of Point-diffraction Interferometers”, *Japan. J. appl. Phys.*, 14, 1-41 (1975). http://dx.doi.org/10.7567/JJAPS.14S1.351

Tunick A.,Tikhonov N., Vorontsov M. and Carhart G., *Characterisation of optical turbulence (Cn2) data measured at the ARL A_LOT facility*, US Army Research Laboratory, (2005).

Weichel H., *Laser Beam Propagation in the Atmosphere*, (Academic, Washington, 1990).